DISSERTATIONES
GEOLOGICAE
UNIVERSITATIS
TARTUENSIS
50

SIGRID SOOMER

Palaeoweathering record of the Archaean–Proterozoic transition in the Imandra–Varzuga Greenstone Belt, north-western Russia

DISSERTATIONES GEOLOGICAE UNIVERSITATIS TARTUENSIS
50

DISSERTATIONES GEOLOGICAE UNIVERSITATIS TARTUENSIS
50

SIGRID SOOMER

Palaeoweathering record of the Archaean–Proterozoic transition in the Imandra–Varzuga Greenstone Belt, north-western Russia

UNIVERSITY OF TARTU
Press
1632

Department of Geology, Institute of Ecology and Earth Sciences, Faculty of Science and Technology, University of Tartu, Estonia.

This thesis is accepted for the commencement of the degree of Doctor of Philosophy in Geology at the University of Tartu on the 11.04.2022 by the Scientific Council of the Institute of Ecology and Earth Sciences, University of Tartu.

Supervisor: Peeter Somelar, Department of Geology, University of Tartu, Estonia

Opponent: Prof. Dr. Heinrich Bahlburg, Institute of Geology and Palaeontology, University of Münster, Germany

This thesis will be defended at the University of Tartu, Estonia, Chemicum, Ravila 14A, room 1019, on the 27th of May 2022 at 13:15.

Publication of this thesis is granted by the Institute of Ecology and Earth Sciences, University of Tartu and by the Doctoral School of Earth Sciences and Ecology created under the auspices of the European Social Fund.

ISSN 1406-2658
ISBN 978-9949-03-872-5 (print)
ISBN 978-9949-03-873-2 (pdf)

Copyright: Sigrid Soomer, 2022

University of Tartu Press
www.tyk.ee

CONTENTS

LIST OF ORIGINAL PUBLICATIONS 6
1. INTRODUCTION 7
2. GEOLOGICAL SETTING 10
3. MATERIALS AND METHODS 14
4. RESULTS 19
   4.1. Petrography, whole-rock mineralogy and geochemistry, and isotope composition of carbonate and organic carbon of the Kuksha palaeoweathering crust 19
   4.2. Mineralogy and whole-rock geochemistry of the Imandra–Varzuga Greenstone Belt metasediments 23
5. DISCUSSION 27
   5.1. Kuksha palaeoweathering crust 27
      5.1.1. Palaeoclimatic interpretation of the Kuksha palaeoweathering 27
      5.1.2. pO_2 and pCO_2 estimation from the composition of the Kuksha palaeoweathering crust 31
   5.2. Provenance and weathering intensity at the transition to oxygenated surface environments as recorded from the Imandra–Varzuga Greenstone Belt metasediments 36
      5.2.1. Tectonic setting and provenance 36
      5.2.2. Weathering intensity 39
6. CONCLUSIONS 44
REFERENCES 46
SUMMARY IN ESTONIAN 57
ACKNOWLEDGEMENTS 60
PUBLICATIONS 61
CURRICULUM VITAE 110
ELULOOKIRJELDUS 111

LIST OF ORIGINAL PUBLICATIONS

This thesis is based on the following published papers. These papers are referred to in the text by their respective Roman numerals.

I Soomer, S., Somelar, P., Mänd, K., Driese, S. G., Lepland, A., Kirsimäe, K. (2019). High-CO_2, acidic and oxygen-starved weathering at the Fenno-scandian Shield at the Archean-Proterozoic transition. *Precambrian Research*, 327, 68–80. https://doi.org/10.1016/j.precamres.2019.03.001

II Somelar, P., Soomer, S., Driese, S. G., Lepland, A., Stinchcomb, G. E., Kirsimäe, K. (2020). CO_2 drawdown and cooling at the onset of the Great Oxidation Event recorded in 2.45 Ga paleoweathering crust. *Chemical Geology*, 548, 119678. https://doi.org/10.1016/j.chemgeo.2020.119678

III Soomer, S., Somelar, P., Mänd, K., Lepland, A., Kirsimäe, K. (2022). Geochemistry and mineralogy of Paleoproterozoic metasediments in the Imandra-Varzuga Greenstone Belt: implications for sediment provenance, tectonic settings and weathering intensity at the transition to oxygenated surface environments. *Precambrian Research*, 371, 106578. https://doi.org/10.1016/j.precamres.2022.106578

The author's contribution:

Paper I: The author was primarily responsible for planning the original research, microscopic and geochemical analysis and data collection. She participated in the interpretation of analytical results, the synthesis of analytical data and the writing of the manuscript.

Paper II: The author was primarily responsible for running experiments, data collection, modelling the data results and contributed to the writing of the manuscript.

Paper III: The author participated in data collection, the interpretation of analytical results, the synthesis of mineralogical-geochemical and analytical data and the writing of the manuscript.

1. INTRODUCTION

The Archaean to Proterozoic transition was manifested by significant environmental disturbances triggered by the shift from anoxic to oxic surface environments during the Great Oxygenation Event (GOE) (Holland, 2006; Lyons et al., 2014), which most probably occurred in successive stages (Holland, 2006; Canfield et al., 2013; Lyons et al., 2014; Poulton et al., 2021). The timing of the GOE is marked by the disappearance of sulphur isotope mass-independent fractionation (MIF) when pO_2 reached values $>10^{-5}$ of Present Atmospheric Level PAL (Luo et al., 2016) dated between 2502 and 2460 million years ago (Ma) (Gumsley et al., 2017; Warke et al., 2020).

The onset of oxidative weathering is thought to have caused an extensive acid attack in weathering environments due to oxidation of sulphide minerals in surface rocks (Holland, 2006). A pulse of acidic weathering and element mobilization following the GOE has been suggested based on Cr-enrichment in Palaeoproterozoic marine iron formations (Konhauser et al., 2011), an increase in weathering intensity and inferred kaolinite richness (Hao et al., 2021) and leaching of phosphorus in early Palaeoproterozoic palaeosols (Hao et al., 2020). Similarly, Mo and U, which are soluble under oxic conditions, show enhanced mobility in Proterozoic palaeosols (Murakami et al., 2016) and occur in elevated concentrations in marine organic-rich Palaeoproterozoic shales (Scott et al., 2008; Partin et al., 2013; Mänd et al., 2020).

However, there is no unequivocal evidence for an increase in chemical weathering indices (e.g. CIA – chemical index of alteration; Nesbitt and Young, 1982) in marine or continental sediments following the GOE. This discrepancy has been explained by limited data availability, while the expected trends are much muted by differences in sediment sources, tectonic-depositional settings, palaeogeography and post-sedimentary alteration between different rock successions (Gaschnig et al., 2014; Li et al., 2016).

Even more importantly, besides the purported effects of atmosphere oxygenation on weathering intensity, the atmospheric carbon dioxide concentration controls Earth's surface temperatures and weathering processes (Kasting, 1987; Dessert et al., 2003; Broecker, 2018). High atmospheric CO_2 concentration lowers the pH of meteoric precipitation and increases the temperature through the greenhouse effect, whereas both phenomena lead to intensified weathering (Kanzaki and Murakami, 2018a, 2018b). Chemical weathering itself has an important impact on the evolution of the Earth's surface environments by regulating atmospheric CO_2 through a negative feedback mechanism (Walker et al., 1981; Kump et al., 2000; Dessert et al., 2003) and release of bio-limiting nutrients into the ocean (Filippelli, 2011; Hao et al., 2017).

Therefore, the palaeosols and palaeoweathering surfaces formed in contact with ancient Earth's surface environments and fine-grained terrigenous sediments derived from weathering crusts are important sources of information on environmental-climatic conditions prevailing at the time of their formation. Palaeosols

are especially valuable for providing insights into terrestrial conditions during times of significant environmental changes.

The Fennoscandian Shield contains several well-preserved palaeoweathering profiles (regoliths and saprolites) developed on the Late Archaean granitoid basement and early Proterozoic metasedimentary-metavolcanic complexes of the Karelian formations (Kirsimäe and Melezhik, 2013). A major unconformity with weathering and denudation at the base of the Palaeoproterozoic sedimentary-volcanic successions was developed on Archaean crystalline basement complexes ca. 2.45 and 2.51 Ga in the Onega and Pechenga basins, respectively (Martin et al., 2013a, 2015). Ojakangas et al. (2001) have suggested that the Archaean–Palaeoproterozoic unconformity detected across the Fennoscandian Shield developed likely as a peneplaned surface on the Archaean rocks isostatically uplifted into a subtropical climate or high-CO_2 environment between 2.4 and 2.2 Ga. The erosion of these rock and sediment suites fed the Karelia–Kola sedimentary basins with weathered terrigenous material that potentially capture the weathering conditions of the time.

The Imandra–Varzuga Greenstone Belt in the northern Fennoscandian Shield, north-western Russia, Kola Peninsula, contains sedimentary units bearing the disappearance of the sulphur isotope MIF signal in the lower part of stratigraphy predating the GOE and the positive carbonate carbon isotope signal of the Lomagundi–Jatuli Event (LJE) following the GOE in its upper part of the stratigraphy (Warke et al., 2020). Therefore, geochemistry of samples from the Greenstone Belt allows testing the weathering intensity changes across the GOE.

This thesis studies the latest Archaean–early Proterozoic weathering conditions using the palaeoweathering crust, the ca. 2.45 Ga Kuksha palaeosol formed on the basaltic parent rock of the Kuksha Volcanic Formation, and the provenance and weathering maturity of the Imandra–Varzuga sediments. The Kuksha palaeosol was formed during the critical time interval just before the change from anoxic to oxic atmospheric conditions, while the Palaeoproterozoic sedimentary record of the Imandra–Varzuga Greenstone Belt contains one of the most complete ca. 2450 and 2000 Ma successions potentially archiving the signatures of the GOE, Huronian global glaciation(s) and the LJE (Karhu and Holland, 1996; Melezhik et al., 1999; Ojakangas et al., 2001).

The main objectives of the thesis are:

- to characterize the Late Archaean–Early Proterozoic (ca. 2.5–2.44 Ga) palaeoweathering crust developed on the basaltic parent rock of the Kuksha Volcanic Formation in the Imandra–Varzuga Greenstone Belt of the Kola Peninsula;
- to model geochemical climofunctions (mean annual temperature, mean annual precipitation) to determine environmental conditions during the formation of the Kuksha weathering crust at the beginning of the GOE;
- to estimate the atmospheric pCO_2 concentrations at the time of the weathering of the Kuksha palaeosol;

– to reconstruct the tectonic settings of deposition, source rock composition (provenance), sedimentary recycling and the degree of chemical weathering of the Imandra–Varzuga metasediments spanning across the Archaean–Proterozoic transition by analysing the changes in silicate weathering intensity related to the atmospheric oxidation of the Palaeoproterozoic.

We propose the hypothesis that the transition from anoxic environment with high pCO_2 to reactive oxic conditions should have increased the weathering intensity. The oxidative weathering is thought to have caused extensive acid attack in weathering environments due to oxidation of sulphide minerals occurring in surface rocks, thus intensifying the weathering process itself.

2. GEOLOGICAL SETTING

The Fennoscandian Shield is a composite craton assembled of different Archaean to Palaeoproterozoic greenstone and orogenic belts comprising metamorphosed igneous and sedimentary rock units (Ojakangas et al., 2001). The north-eastern part of the Fennoscandian Shield includes the Imandra–Varzuga Greenstone Belt, a south-eastern segment of the ca. 800-km-long system of supracrustal belts (Melezhik, 1996) extending from northern Norway and Finland to the Kola Peninsula in north-western Russia (Figure 1). The 350-km-long and up to 10–50-km-wide Imandra–Varzuga Greenstone Belt (Chashchin et al., 2008) has been interpreted as a rift system which initiated around 2.5 Ga and was abandoned and reactivated several times through the Palaeoproterozoic (Melezhik, 2013). The major periods of tectonic activity of this belt are recorded at 2.44, 2.2, 2.1 and 1.97 Ga (Nykänen et al., 1994; Ojakangas et al., 2001).

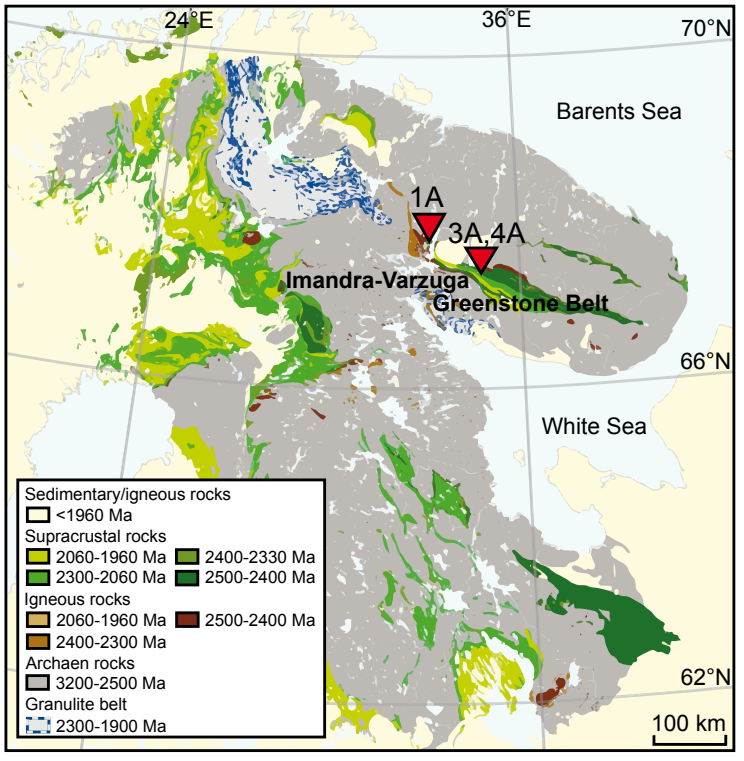

Figure 1. *Locations of cores 1A, 3A and 4A (denoted with red arrows) on the western flank of the Imandra–Varzuga Greenstone Belt. Modified after Melezhik et al. (2013).*

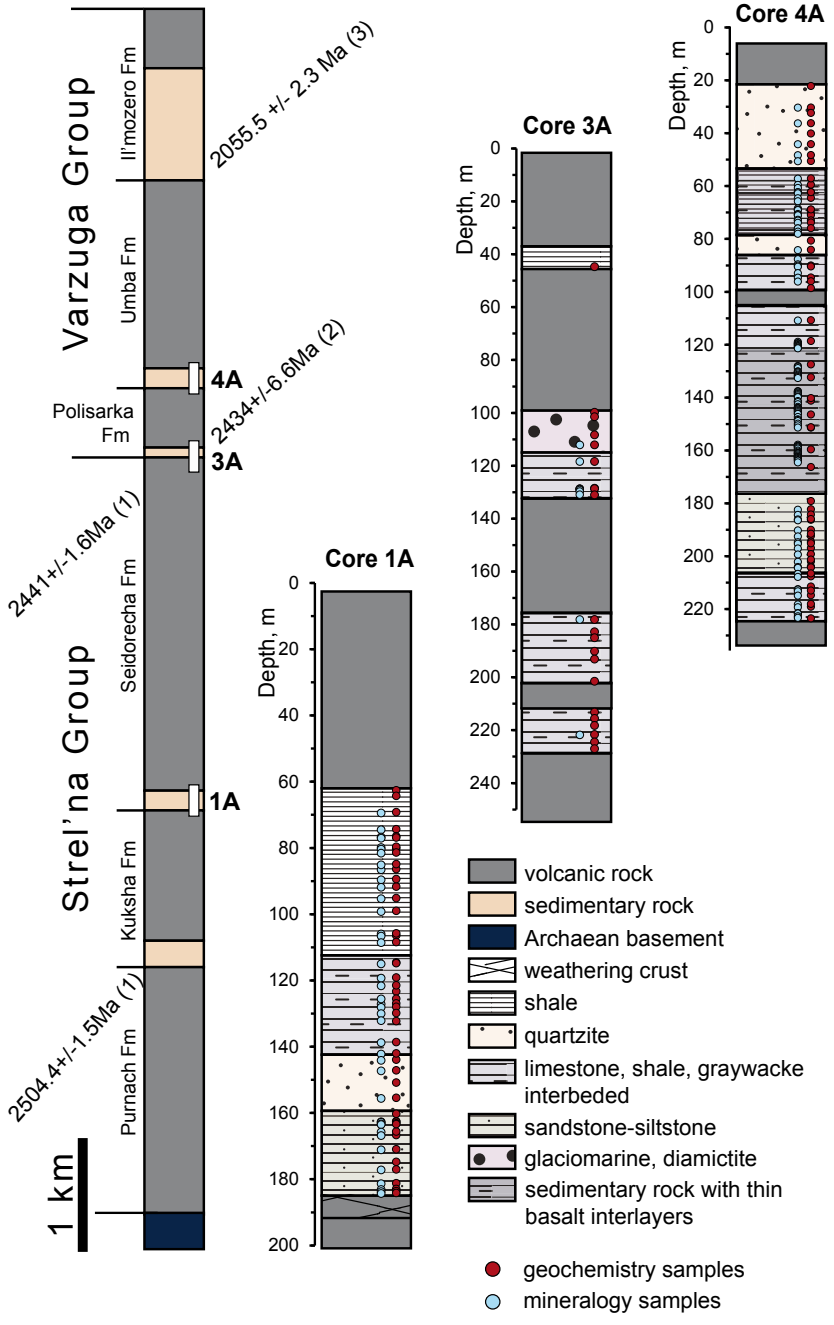

Figure 2. *Stratigraphy and simplified lithology of the Strel'na and Varzuga groups with the studied core intervals and the location of the sampling points: mineralogy (blue) and geochemistry (red). References to dates are as follows: 1, Amelin et al. (1995); 2, Brasier et al. (2013); 3, Martin et al. (2013a).*

The Imandra–Varzuga Supergroup is subdivided into the Strel'na, Varzuga and Tominga groups (Melezhik, 2013; Figure 2). The Strel'na Group comprises, from base to top, the Purnach Formation tholeiitic basalts interlaced with sandstones that are resting unconformably on the Archaean crystalline basement; the sandstone-greywacke-conglomerates of the Kuksha Sedimentary Formation and tholeiitic basalts of the Kuksha Volcanic Formation; greywacke-shale and sandstones of the Seidorechka Sedimentary Formation, and lavas and tuffs of the Seidorechka Volcanic Formation (Melezhik et al., 2013).

The overlying Varzuga Group is represented by three sedimentary-volcanic units – the Polisarka Sedimentary and Volcanic formations, the Umba Sedimentary and Volcanic formations and the Il'mozero Sedimentary and Volcanic formations (Melezhik, 2013). The Polisarka Sedimentary Formation is characterized by polymict conglomerates, diamictites, varved siltstones with dropstones, shales, marls and limestones followed by submarine volcanics including pillowed lavas of the Polisarka Volcanic Formation. The diamictites of the Polisarka Sedimentary Formation have been correlated with the Huronian glaciation (Ojakangas et al., 2001; Melezhik, 2013; Gärtner et al., 2014; Warke et al., 2020). The Umba Sedimentary Formation consists of greywacke, sandstone-siltstone, shale, dolostone and limestone.

The Umba Volcanic Formation is represented mainly by subaerial subalkaline to alkaline basalts and tuffs emplaced in intracratonic rift settings (Melezhik, 2013). The Il'mozero Sedimentary and Volcanic formations are mainly turbiditic greywackes, black shales with subordinate carbonate rocks and mafic tuffs, and basaltic andesite lava flows, respectively (Melezhik, 2013).

The Varzuga Group is succeeded by the stratigraphically poorly defined Tominga Group that consists of volcaniclastic greywacke, sandstones, schists, carbonate rocks, tholeiitic pillow basalts, andesites, dacites and rhyolites (Melezhik, 2013).

The Kuksha palaeosol is described in the Imandra–Varzuga Supergroup, in the Strel'na Group on top of the Kuksha Volcanic Formation and is overlaid by the sediments of the Seidorechka Sedimentary Formation (Melezhik et al., 2013).

The maximum depositional age of the Imandra–Varzuga sedimentary successions is constrained by zircon U–Pb ages 2501.5 ± 1.7 and 2504.4 ± 1.5 Ma of gabbronorite intrusions into the Kuksha Sedimentary Formation (Amelin et al., 1995). The upper age of the Seidorechka Sedimentary Formation is constrained by the synvolcanic bodies of granophyre "imandrites" in the overlying Seidorechka Volcanic Formation where baddeleyite and zircon U–Pb ages are dated as 2442.2 ± 1.7 and 2441 ± 1.6 Ma, respectively (Amelin et al., 1995). These also define the age of the Kuksha palaeoweathering, suggesting that the maximum weathering duration of the Kuksha weathering crust was ca. 60 Ma.

The Polisarka Volcanic Formation has been dated by zircon U–Pb age at 2434 ± 6.6 Ma (Brasier et al., 2013) and is further constrained by Warke et al. (2020) who delimited the depositional age of the Seidorechka Sedimentary Formation between 2501.5 ± 1.7 and 2441 ± 1.6 Ma, and the Polisarka Sedimentary Formation between 2441 ± 1.6 and 2434 ± 6.6 Ma. However, detrital zircon

U–Pb ages place the depositional age of the Seidorechka Sedimentary Formation to around 2430 Ma, and the deposition of glacigenic rocks of the Polisarka Sedimentary Formation to around 2411 Ma (Gärtner et al., 2014).

The depositional age of the Umba Sedimentary Formation is poorly constrained. The maximum age is defined by the aforementioned stratigraphically older Polisarka Volcanic Formation. The minimum age is given by the maximum depositional age of the stratigraphically younger Il'mozero Sedimentary Formation at 2055.5 ± 2.3 Ma by Pb–Pb ages of detrital zircons that are considered to be derived from the Umba Volcanic Formation and thereby defining its age (Martin et al., 2013a).

Carbonates in the Umba Sedimentary Formation are characterized by positive $\delta^{13}C$ values as high as +6.7‰ (Melezhik and Fallick, 1996), typical of the Lomagundi–Jatuli Event (LJE). Given that the onset of the LJE has been between 2306 ± 9 and 2221 ± 5 Ma (Martin et al., 2013b), the deposition of the Umba Sedimentary Formation could have occurred at some point between 2306 ± 9 and 2055.5 ± 2.3 Ma. The minimum age constraint is consistent with the age of the stratigraphically coeval Kuetsjärvi Volcanic Formation in the Pechenga Greenstone Belt – 2058 ± 6 Ma by Melezhik et al (2013) and 2056.6 ± 0.8 Ma by Martin et al (2013a).

The Imandra–Varzuga greenstone successions are overprinted by greenschist facies metamorphism locally reaching amphibolite facies conditions at 2202 ± 17 Ma, as suggested by titanite and rutile ages in the Seidorechka Volcanic Formation (Chashchin et al., 2008).

3. MATERIALS AND METHODS

The material studied was sampled from cores 1A, 3A and 4A that were drilled in 2007 during the International Fennoscandian Arctic Russia – Drilling Early Earth Project (FAR-DEEP) (Melezhik, 2013). Thirty-two samples from core 1A were used for the palaeoweathering research of the Kuksha palaeosol (Papers I and II), and altogether 182 samples were employed for the analysis of terrigenous sediments (Paper III). The terrigenous sediment lithologies in drill cores 1A, 3A and 4A were discriminated using Herron's geochemical classification (Herron, 1988) where the log(Si/Al) threshold 0.7 for defining shales and siltstones was used, instead of 0.6 as originally proposed by Herron (1988).

Fifteen 2 cm × 3 cm uncovered petrographic thin sections were analysed to characterize the changes in the mineralogy and pedogenic structure of the early Palaeoproterozoic weathering crust. Thin sections were studied both in plane-polarized light (ppl) and cross-polarized light (xpl) using an Olympus BX51 petrographic microscope at Baylor University, U.S.A. To determine mineral alteration, selected thin sections and polished slabs representing characteristic lithologies from the parent basalt to strongly weathered intervals were examined under the scanning electron microscope (SEM) using a ZEISS EVO MA15 SEM equipped with Oxford AZTEC-MAX energy-dispersive (EDS) system.

The whole-rock mineralogy of the samples was studied in powdered, randomly oriented samples by means of X-Ray diffraction (XRD). The XRD patterns were measured using a Bruker D8 Advance diffractometer in the 2–70° 2Θ range. The quantitative mineralogical composition was interpreted and modelled using the Rietveld algorithm-based program Siroquant-3 (Taylor, 1991).

The whole-rock chemical composition, minor and trace element contents were analysed in three sample sets. "FAR-DEEP" archive samples were measured at the Geological Survey of Norway with a Philips PW 1480 X-ray fluorescence (XRF) spectrometer. For major elements, Li-borate fused beads were prepared, whereas minor elements were measured from pressed powder pellets. The detection limits for major elements were generally below 0.02% and the typical precision (1σ) was ~2%. For minor elements, detection limits were ≤10 μg g^{-1}. The XRF spectrometer was calibrated using a set of ~120 internationally certified natural rock standards as well as ~20 artificial standards provided by the XRF manufacturer.

The chemical composition of samples was analysed in ACME Laboratories, Bureau Veritas Commodities Canada Ltd., via inductively coupled plasma optical emission and mass-spectroscopy (ICP-OES/ICP-MS) from aliquots fused into a $LiBO_2$ beads. Minor elements were digested using a mix of HNO_3, $HClO_4$ and HF and analysed via inductively coupled plasma mass spectrometry (ICP-MS). The average relative standard deviation was less than 5% for all elements; accuracy was monitored using OREAS 25a and OREAS 45e reference materials.

Element concentrations were measured at the Department of Geology, University of Tartu, by using digested mix of HNO_3, $HClO_4$ and HF and analysed via ICP-MS Agilent 8800. External accuracy was assessed by measuring the

geostandard BHVO-2, which showed a <10% relative difference between measured and known values for all elements.

The $\delta^{18}O$ and $\delta^{13}C$ values were measured from micro-drilled samples of calcite and siderite using a Thermo Fisher Scientific Delta-V-Advantage, continuous-flow isotope gas-ratio mass-spectrometer, with an analytical precision (2σ) of 0.1‰, which was coupled with Gas Bench II. For carbonate $\delta^{13}C$ analysis samples were kept at 50 °C for 24 h in 99% ortho-phosphoric acid (H_3PO_4) for calcite (and dolomite) dissolution. Thereafter samples were flushed with He for 5 min and siderite was then dissolved at 70 °C for 72 h in ortho-phosphoric acid. The reproducibility of repeated analyses was better than ±0.1‰ for $\delta^{18}O$ and ±0.2‰ for $\delta^{13}C$.

The $\delta^{13}C$ values of organic carbon in the uppermost part of the palaeoweathered profile were measured by the Delta-V Plus instrument connected with a Finnigan Flash HT via ConFlo IV in samples decarbonated with 10% v/v HCl. The measured amount of organic carbon in the gas was below 0.2% and the reproducibility of repeated organic carbon analyses was better than ±0.5‰ for $\delta^{13}C$. The results are expressed in per mil deviation relative to the Vienna Peedee Belemnite (VPDB) scale for oxygen and carbon.

Mineralogical trends and chemical variability of the palaeoweathering profile and siltstone-shale lithologies in the Seidorechka, Polisarka and Umba Sedimentary formations of the Imandra–Varzuga Greenstone Belt were analysed for determining the weathering rate, and gains and losses of mobile elements. The chemical index of alteration (CIA, Eq. (1)) (Nesbitt and Young, 1982), the chemical index of alteration minus potassium (CIA – K, Eq. (2)) (Maynard, 1992), the mafic index of alteration ($MIA_{(R)}$, Eq. (3)), the mafic index of alteration minus potassium ($MIA_{(R)}$ – K, Eq. (4)) and the weathering index of Parker (WIP, Eq. (5); Parker, 1970) were used. All the indices were calculated using molar proportions:

$$\mathrm{CIA} = \left(\frac{Al_2O_3}{Al_2O_3+Na_2O+K_2O+CaO^*}\right)\cdot 100 \quad (1)$$

$$\mathrm{CIA}-\mathrm{K} = \left(\frac{Al_2O_3}{Al_2O_3+Na_2O+CaO^*}\right)\cdot 100 \quad (2)$$

$$\mathrm{MIA_{(R)}} = \left(\frac{Al_2O_3}{Al_2O_3+Fe_2O_{3(Total)}+MgO+CaO^*+Na_2O+K_2O}\right)\cdot 100 \quad (3)$$

$$\mathrm{MIA_{(R)}}-\mathrm{K} = \left(\frac{Al_2O_3}{Al_2O_3+Fe_2O_{3(Total)}+MgO+CaO^*+Na_2O}\right)\cdot 100 \quad (4)$$

$$\mathrm{WIP} = \left(\frac{2\cdot Na_2O}{0.35}+\frac{MgO}{0.9}+\frac{2\cdot K_2O}{0.25}+\frac{CaO^*}{0.7}\right)\cdot 100 \quad (5)$$

In these equations CaO* represents molar proportions of CaO bound into silicate minerals. The CaO* correction was done using the method of McLennan et al. (1993) (see for details Soomer et al., 2022 – PAPER III).

Mass-balance (τ) calculations for the Kuksha palaeoweathering crust were performed according to Brimhall and Dietrich (1987), where the concentrations (C) of particular elements (j) in the parent rock (p) and in weathered material (w) are normalized vs. an immobile element such as titanium (Ti) (Eq. (6)):

$$\tau_j = \left(\frac{\frac{C_{jw}}{C_{jp}} / C_{Tiw}}{C_{Tip}} \right) - 1 \quad (6)$$

To estimate the palaeo-pH values, an AlCa geochemical proxy (Eq. (7)) developed by Lukens et al. (2018) was used:

$$\mathrm{AlCa} = \left(\frac{Al_2O_3}{Al_2O_3 + CaO} \right) \cdot 100 \quad (7)$$

For mean annual precipitation (MAP) estimates, two different methods were used. The first was the relationship between CIA – K and MAP (Eq. (8)) by Sheldon et al. (2002), in which the standard error is ±172 mm yr^{-1} and R^2 is 0.73 for the empirical fit:

$$\mathrm{MAP} = 221 e^{0.0197(\mathrm{CIA-K})} \quad (8)$$

The palaeosol-palaeoclimate model PPM1.0 (Stinchcomb et al., 2016) was also used because it offers a more data-driven modelling approach using a wider variety of soil types compared to CIA – K.

For mean annual temperature (MAT) estimates, the equations based on the salinization index and clayeyness molecular ratios were used, along with the output from PPM1.0. The relationship between MAT and salinization (Eq. (9)) was from Sheldon et al. (2002), where the standard error is ±4.4 °C, R^2 is 0.37 and $S = (K_2O + Na_2O)/Al_2O_3$:

$$\mathrm{MAT} = -18.5 \times S + 17.3 \quad (9)$$

The relationship between MAT and clayeyness (Eq. (10)) is from Sheldon (2006), where the standard error is ±0.6 °C, R^2 is 0.96 and $C = Al_2O_3/SiO_2$:

$$\mathrm{MAT} = 46.94 \times C + 3.99 \quad (10)$$

Palaeoatmospheric pCO_2 was estimated using the Sheldon (2006) method (Eq. (11)), which evaluates total mass flux for CaO, MgO, Na_2O and K_2O_{CALC} (described in Medaris et al., 2015, 2018) during weathering. The calculation assumes the parameters other than weathering duration remain constant during the weathering period:

$$\frac{M}{t} \approx pCO_2 \left(\frac{K_{CO2} r}{10^3} + \frac{\kappa D_{CO2} \alpha}{L}\right) \quad (11)$$

Here M/t represents time-averaged flux of CO_2 required for the observed weathering (mol cm^{-2} yr^{-1}). Its value depends on pCO_2 – the partial pressure of atmospheric CO_2 (atm), K_{CO2} – the Henry's Law constant for CO_2, r – the rainfall rate (cm yr^{-1}), κ – a unit-conversion constant (1.43 × 103 s cm^3 mol^{-1} yr^{-1}) equal to seconds in a year divided by the molar volume of gas at standard temperature and pressure, D_{CO2} – the diffusion constant for CO_2 in air (0.162 cm^2 s^{-1}) with α being the ratio of the diffusion constant for CO_2 in soil divided by that in air and L – the depth to the water table. We follow Sheldon (2006) in taking values of 0.034 mol atm^{-1} for K_{CO2}, 0.1 for α and an average of 100 cm yr^{-1} for the rainfall rate r, depending on our MAP estimations using the CIA – K geochemical proxy of Sheldon et al. (2002) and the PPM1.0 model of Stinchcomb et al. (2016). Depth to the water table (L) was placed at the saprolite-unweathered (or least-weathered) protolith (or saprock) contact at 2 m. Estimates for the decompaction of the soil were not used, as this unknown parameter would increase the uncertainties in the outcome.

Additionally, the palaeoatmospheric CO_2 concentrations were estimated by assuming the isotopic equilibrium between $\delta^{13}C$ pedogenic carbonate and soil CO_2 (Eq. (12)):

$$CO_{2(atm)} = S(z) \frac{\delta^{13}C_s - 1.0044\,\delta^{13}C_r - 4.4}{\delta^{13}C_a - \delta^{13}C_s} \quad (12)$$

Here S(z) is the contribution of soil-respired CO_2 as a function of depth (z); C_s, C_r and C_a are $\delta^{13}C$ of soil CO_2 (calculated from pedogenic carbonate), soil-respired CO_2 (measured from organic matter) and atmospheric CO_2, respectively (Royer et al., 2001). For atmospheric CO_2 (C_a) we used a $\delta^{13}C$ value of –6.5‰, as suggested by Friedli et al. (1986). The pCO_2 estimates are vs. present atmospheric level (PAL) CO_2 levels of 300 ± 10 ppm, as were used in other previous studies (Lowe and Tice, 2004; Sheldon, 2006; Driese et al., 2011; Kanzaki and Murakami, 2015). Commonly the carbonate-based pCO_2 estimates are based on calcite $\delta^{13}C$ values, but some authors (Tabor et al., 2004; Feng and Yapp, 2009) use an analogous proxy based on the ferric carbonate [$Fe(CO_3)(OH)$] component in goethite.

In addition, the sediment protolith composition and weathering intensity of the fine-grained shale and shale-siltstone lithologies were simultaneously estimated using a recent modelling approach developed by Lipp et al. (2020). They use the centred log-ratio transformed composition (Aitchison, 1986) of major oxides (SiO_2, Al_2O_3, Fe_2O_3, MgO, Na_2O, CaO, K_2O) where x' is expressed as the sum of a weathering vector, ŵ, and a protolith vector, $\hat{\mathbf{p}}$ – both calculated using an R script by Lipp et al. (2020, 2021) – relative to the composition of the upper continental crust (UCC, Rudnick and Gao, 2014):

$$x' = UCC + \omega\hat{w} + \psi\hat{p} + E \quad (13)$$

The coefficients of these vectors correspond to the weathering intensity experienced by sediment, ω, and its protolith composition, ψ, whereas E is the misfit from the model (Lipp et al., 2020). Compared with the modern UCC the positive or negative ψ values reflect more or less felsic composition for sediment protolith, respectively. A Ca correction was applied according to the screening criteria given by Lipp et al. (2021). Lipp et al. (2021) suggested that the protolith of the Archaean sediments was more dacitic in composition than the modern UCC. We tested the influence of the suggested Archaean protolith on the ω and ψ values of the studied sediments; however, the differences from the estimates using the modern UCC as a protolith are insignificant.

Europium (Eu) and cerium (Ce) anomalies in rare earth element (REE) patterns were calculated on deviations from predicted values, as derived from the chondrite-normalized (CN) abundances of neighbouring elements (Eqs (14) and (15)):

$$\frac{\mathrm{Eu_{CN}}}{\mathrm{Eu^{*}_{CN}}} = \frac{\mathrm{Eu_{CN}}}{\mathrm{Sm_{CN}} + \mathrm{Gd_{CN}}/2} \tag{14}$$

$$\frac{\mathrm{Ce_{CN}}}{\mathrm{Ce^{*}_{CN}}} = \frac{\mathrm{Ce_{CN}}}{\mathrm{La_{CN}} + \mathrm{Pr_{CN}}/2} \tag{15}$$

4. RESULTS

4.1. Petrography, whole-rock mineralogy and geochemistry, and isotope composition of carbonate and organic carbon of the Kuksha palaeoweathering crust

The transition from the palaeoweathering crust on top of the Kuksha Volcanic Formation to the overlying sandstone-siltstone and shale (greywacke) of the Seidorechka Sedimentary Formation is marked by an undulating erosional surface. Weathered, redeposited material just above the palaeoweathering crust surface consists of chlorite, K-mica with some quartz and plagioclase, with trace amounts of pyrite, titanite, ilmenite, and rare earth element (REE) carbonates and REE-phosphates. The weathered upper part of the Kuksha Volcanic Formation is mottled, characterized by dark greenish-grey and light grey chlorite-mica and calcite-quartz patches and is crosscut by calcite and quartz veins. At a depth of 2.8 m below the palaeoweathering surface the rock changes to more equally distributed small lighter and darker patches, and further down the rock becomes homogenously grey, with only slight hints of green (Figure 3). About 5.5–6 m below the palaeoweathering surface the alteration of the basalt is recognized only along the joints until the end of the profile (Soomer et al., 2019 – PAPER I).

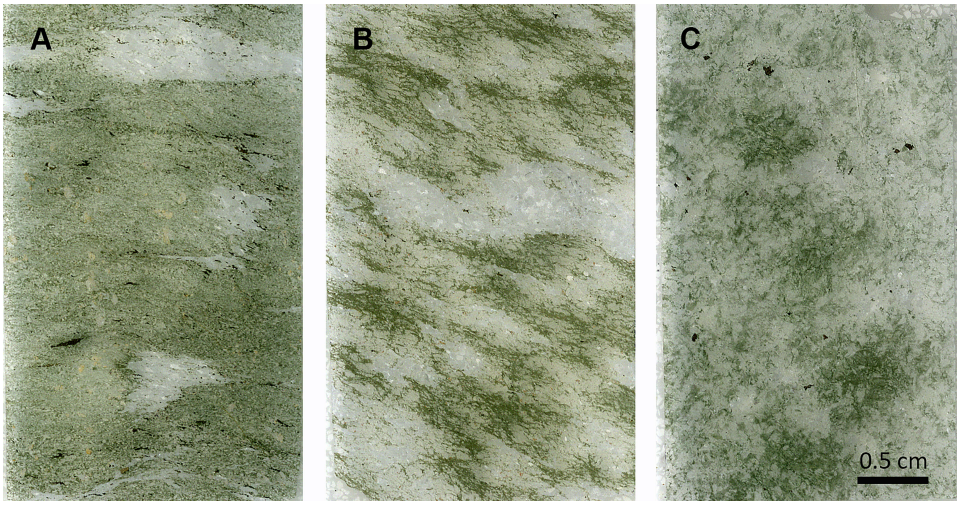

Figure 3. *The appearance and texture of the Kuksha palaeoweathering crust in thin-section samples in ordinary incident light. (A) intensely weathered rock at 1.8 m below the weathering surface, (B) less altered rock at 5.2 m depth, (C) least altered parent rock appearance at 11.5 m depth.*

The upper 1.5 m of the palaeoweathering crust is characterized by the appearance of siderite and kaolinite polymorph dickite (Figure 4). Siderite and dickite show a gradual increase towards the top of the weathered section to ca. 17 and 7 wt%, respectively. Siderite occurs at contacts with pyritic aggregates and as a cement, whereas dickite is found as irregular to slightly plate-like grains. The matrix of the weathered rock is composed of chlorite and K-mica intercalated by areas of recrystallized quartz. Also, euhedral zircons and REE-phosphate, possibly rhabdophane [(La, Ce, Nd) PO_4 nH_2O] aggregates occur (Soomer et al., 2019 – PAPER I).

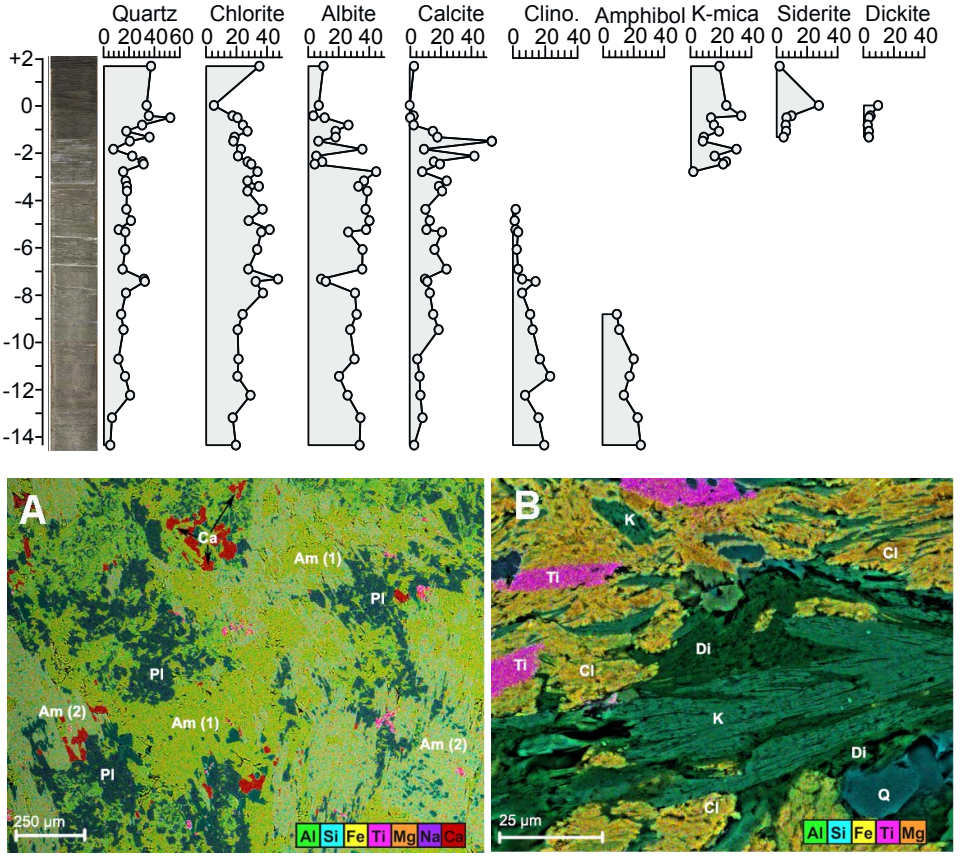

Figure 4. *Changes in the mineralogy of the palaeoweathering profile with depth (relative to the weathering surface). There is no dickite in the overlying sediments, and siderite is absent above the zone probably representing the redeposited weathering crust. Clino. – Clinozoisite, Amp. – Amphibolite. (A) EDS layered image of the parent rock. The main mineral phases in the parent rock are represented by two types of amphibole – nearly stoichiometric hornblende [Am (1)] and Ca, Si-depleted, Fe, Al-enriched variety [Am (2)] together with plagioclase (Pl) and calcite (Ca) at 13 m depth below the weathering surface, and (B) of dickite (dark green, Di) intergrown with K-mica (lighter green, K) in the matrix of a mixture of siderite (Sid), chlorite (yellow, Cl) and K-mica lamella intersected by rare titanite crystals (pink, Ti) and quartz grains (blue, Q) at the very top of the palaeoweathering crust (depth 185.79 m).*

Chlorite, mica, albite, quartz and titanite are found in the deeper part of the weathered profile (ca. 2 m below the weathered surface). The least weathered parent rock at a depth of 14 m below the weathered surface consists of amphibole, plagioclase, chlorite, clinozoisite and calcite, with minor quartz and titanite. Amphibole occurs in two different compositions, hornblende and a Ca and Si-depleted but Fe and Al-enriched phase that, along with chlorite and clinozoisite, indicate at least partial weathering and/or hydrothermal overprinting in the parent basalt. The results of XRD analysis (Soomer et al., 2019 – PAPER I) indicate that amphibole and clinozoisite disappear at depths of 9 and 4 m below the weathered surface, respectively. K-mica appears and plagioclase shows about a two-fold decrease from around 30 to 15 wt% at a depth of about 3 m below the weathering surface (Figure 4).

Calcite is a common phase throughout the succession showing a significant increase at depths between 1.5 and 2 m below the weathering surface but is nearly absent in the uppermost part of the weathering profile. Also, the quartz content rises from 10–15 wt% in the bottom of the core to around 30–35 wt% at the top of the weathering surface. Chlorite is one of the prevalent phases (up to 40 wt%) in the middle of the weathered interval.

The results of the whole-rock XRF analyses were used for the calculations of mass-balance and weathering indices (Soomer et al., 2019 – PAPER I). Mass-balance calculations of major oxides, normalized to Ti, have values similar to slightly altered parent rock compositions up to 3 m below the weathered surface while above Na, Ca, Mg are progressively depleted, and P is enriched. Si and Fe display minor enrichment in the uppermost weathered zone. In contrast to the other alkali elements, with respect to the parent rock, K is strongly enriched in the weathering crust, showing enrichment over 100% in the interval above 2.5 m depth and reaching values over 200% in the uppermost part of the weathered section.

The CIA values increase from about 47 in the lower part of the profile to as high as 85 in the uppermost 1.5 m of the profile in the weathering crust, whereas CIA – K values reach up to 91 in the same interval (Figure 5; Soomer et al., 2019 – PAPER I). The values of the $MIA_{(R)}$ and $MIA_{(R)}$ – K increase from around 25 up to 42 for the $MIA_{(R)}$ and 25–46 for $MIA_{(R)}$ – K from parent rock to the most weathered rock, respectively. The A–CNK–FM plot shows a typical weathering trend with losses of Ca, Na, Mg and Fe along with accumulation of Al (see Figure 9A in Soomer et al., 2019 – PAPER I). Compared to parent rock, the uppermost part of the weathering crust shows Ba enrichment and Sr depletion with Ba/Sr ratio reaching >10. The provenance proxy, expressed as the Ti/Al molar ratio, has very low values typical for basaltic rocks that remain unchanged throughout the profile (0.035 ± 0.005), which suggests a uniform mafic parent rock of the weathering profile.

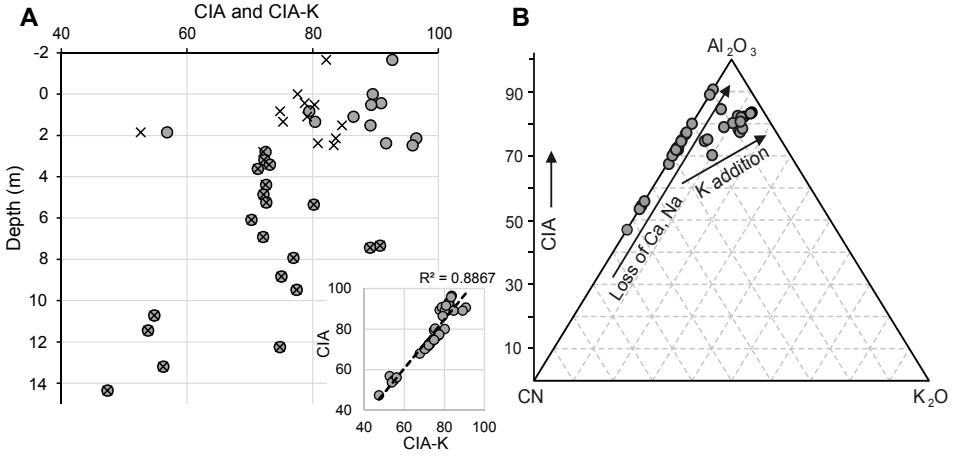

Figure 5. *(A) Comparative CIA (denoted by x) and CIA – K (denoted by a dot) displaying a K-metasomatic overprint. The correlation over the shown profile between the CIA and CIA – K is $R^2 = 0.89$ ($p < 0.05$). (B) The A-CN-K triangular plot and overall CIA values. The parent rock values are in the range of gabbro-basalt, whereas the weathered upper part of the palaeoweathering crust is shifted towards the illite composition (Al_2O_3–K_2O line), showing K addition.*

Leaching effects under oxygenated conditions were evaluated with V/Al and V/Ti ratios that show nearly constant values over the profile, while the Cr/Ti ratio varying mostly between 0.023 and 0.039 shows lower values (0.017–0.018) in the uppermost part of the profile. Also, both U and Th are enriched in the upper part of the weathering crust, with U showing stronger enrichment as the U/Th ratio increases from 0.15 in the lower part of the profile to 0.2–0.4 in the uppermost 2 m of the palaeoweathering crust with a distinct maximum of 0.6–0.7 at 1 m below the weathering surface (Soomer et al., 2019 – PAPER I).

Two siderite samples from the uppermost 1.5 m thick part of the Kuksha palaeoweathering profile give $\delta^{13}C$ values of –0.6‰ and –3.3‰ (Somelar et al., 2020 – PAPER II). Calcite appearing below the siderite zone shows an increase in $\delta^{13}C$ values from –8.9‰ at 1.8 m below the palaeoweathered surface to –4.7‰ at 14 m depth. Trace amounts of organic carbon (0.22–0.04 wt%) detected in the upper part of the Kuksha palaeoweathering profile have $\delta^{13}C$ values from –21.8‰ to –23‰ in samples with siderite in the uppermost 1.5 m thick part of the profile, and –26.9‰ to –28.5‰ at depths of 2–4 m below the palaeoweathered surface (Somelar et al., 2020 – PAPER II).

4.2. Mineralogy and whole-rock geochemistry of the Imandra–Varzuga Greenstone Belt metasediments

The Seidorechka Sedimentary Formation is the stratigraphically oldest unit studied in the Imandra–Varzuga Greenstone Belt (Figure 2). This unit is represented by the shale-siltstone, limestone-shale and sandstone succession in drill core 1A, characterized by a quartz, plagioclase feldspar and phyllosilicate (chlorite and K-mica) assemblage with varying amounts of carbonate phases (calcite and dolomite), minor titanite, ilmenite and sulphides (Figure 6; Soomer et al., 2022 – PAPER III). Quartz content is higher in the lower part of the succession, reaching about 80 wt% in the Quartzite Member and decreasing to <20% in the uppermost part of the Shale Member. The plagioclase feldspar increases opposite to quartz gradually from 5–10 wt% in shale-siltstones of the lower part of the succession to ca. 30–40 wt% in the Shale Member. K-mica and chlorite are the major phyllosilicates (ca. 30–60 wt%) but reach 80 to nearly 100 wt% in some samples of the Shale Member. Calcite and/or dolomite content is low (<5%) except in the Limestone-Shale Member and in a <1 m thick carbonate bed defined as the Dolostone Member (Melezhik et al., 2013) where the maximum values are 16 and 46 wt%, respectively (Soomer et al., 2022 – PAPER III).

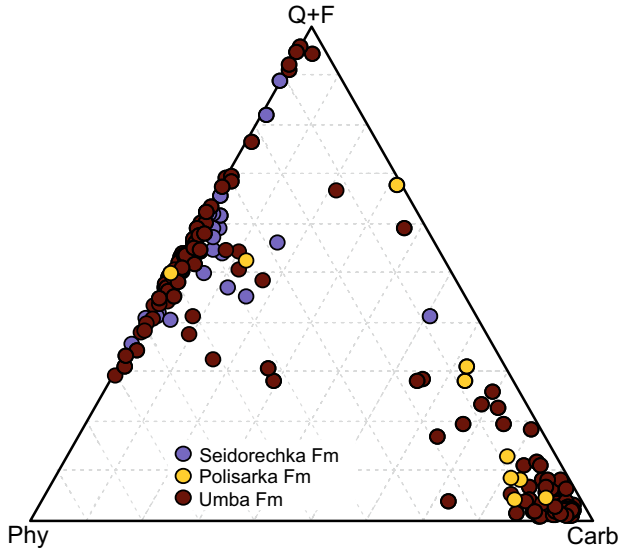

Figure 6. *The mineralogical composition of samples obtained from the sedimentary successions of three cores: A1 – Seidorechka Sedimentary Formation (blue dots), A3 – Polisarka Sedimentary Formation (yellow dots), A4 – Umba Sedimentary Formation (brown dots). Q + F = Quartz + Feldspar, Phy = phyllosilicates, Carb = Carbonates. Note that the more siliciclastic samples that are later selected for further analysis are plotting at the Q + F – Phy line.*

The Greywacke-Diamictite and Limestone members of the Polisarka Sedimentary Formation in drill core 3A are mainly characterized by quartz-feldspar-phyllosilicate and calcite/dolomite assemblages, respectively. The quartz content in greywacke is ca. 25–30 wt%, plagioclase feldspar ca. 20 wt% with 20–30 wt% K-mica and ca. 15 wt% chlorite. The calcite content in carbonate rocks of the Limestone Member varies from 32 to 80 wt% (Soomer et al., 2022 – PAPER III).

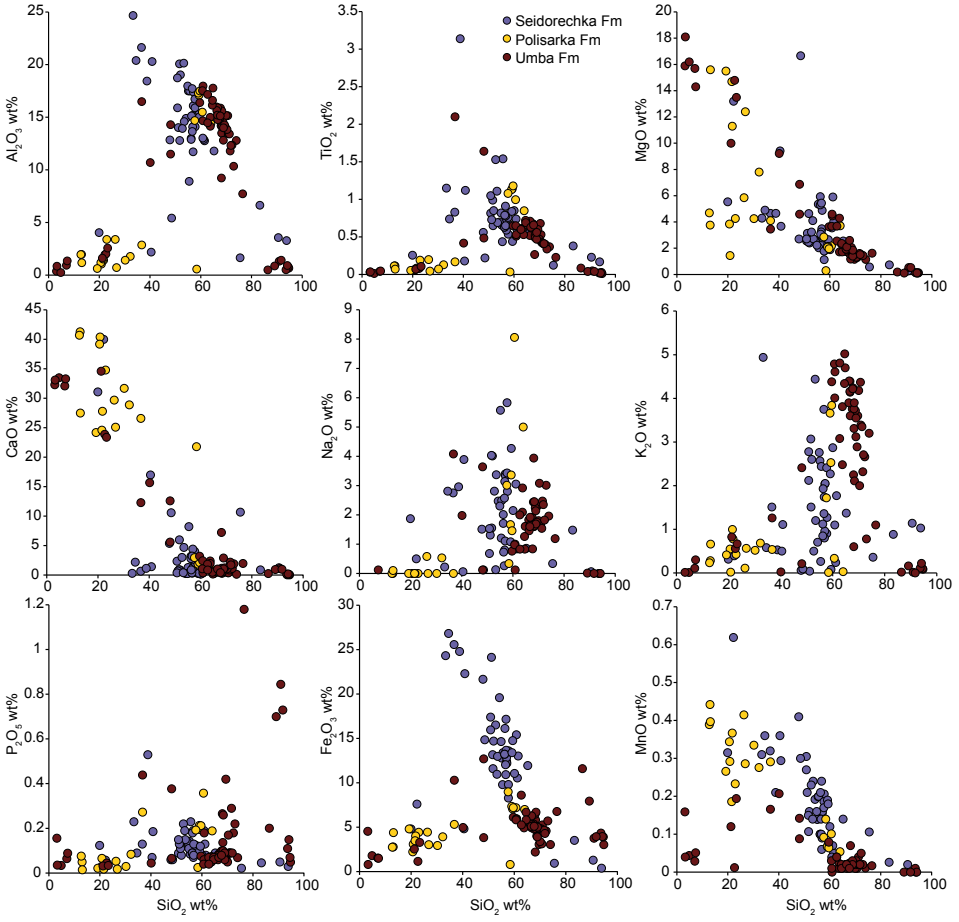

Figure 7. *Variation diagrams characterizing major element composition against SiO_2 in all cores.*

The Umba Sedimentary Formation in drill core 4A is divided (from top to bottom) into the Quartzite, Shale, Dolostone and Sandstone-Siltstone members. The Quartzite Member has a quartz content >85 wt%. The Shale Member is dominated by phyllosilicates typically with a content from 30 wt% to nearly 70 wt% and quartz (15–51 wt%), and minor K-feldspar/plagioclase. The dolomite content in the Dolostone Member is commonly >65 wt% with calcite mostly between 5 and 25 wt%. Shale beds in the Dolostone Member are characterized by K-mica, quartz and feldspar. In the Sandstone-Siltstone Member quartz,

K-feldspar and plagioclase make about 40–70 wt% and phyllosilicates (mainly K-mica) 25–49 wt%. Dolomite and calcite are found in the carbonate-rich beds in the lower part of the member.

The chemical composition of the studied formations corresponds to their mineral composition (Figure 7). According to Herron's geochemical classification of siliciclastic sediments (Herron, 1988), most of the selected samples represent shales and Fe-shales, and wackes with some quartz arenites (Figure 8).

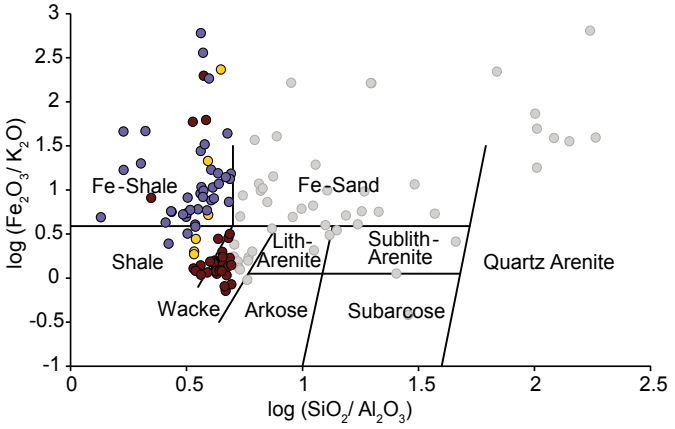

Figure 8. *Siliciclastic sediment classification (modified after Herron, 1988) for the terrigenous sediments of the Seidorechka Sedimentary Formation (blue dots), A3 – Polisarka Sedimentary Formation (yellow dots), A4 – Umba Sedimentary Formation (brown dots). Herron classification was used for selecting out the shale and wacke samples for further analysis.*

The trace element composition of the shales and siltstone-shales present in the Seidorechka Sedimentary and Umba Sedimentary formations is depleted with respect to Post-Archaean Australian Shale (PAAS) (Taylor and McLennan, 1985) in large ion lithophile (LIL) elements Rb, Sr and Cs (but not in Ba), and in high field strength elements (HFSEs), such as Th, Nb and U except Zr showing values around PAAS (see Figure 6a, b, c in Soomer et al., 2022 – PAPER III). Mo, Cr, Co, Ni and Sc are slightly enriched in the Seidorechka Sedimentary Formation but somewhat depleted in the Umba Sedimentary Formation shales, indicating selective loss of the oxygen-sensitive elements in the Umba Sedimentary Formation sediments. Also, the shales of the Seidorechka Sedimentary Formation have higher mean values of transition elements like Cr, Co and Ni, whereas the average V content of both formations is similar to PAAS. The chondrite-normalized REE patterns (Taylor and McLennan, 1985) of selected representative shales of the Seidorechka and Umba Sedimentary formations (Figure 9) show different distribution patterns. The shales in the Seidorechka and Umba Sedimentary formations show fractionation and enrichment of light rare earth elements (LREE) expressed by chondrite-normalized (CN) La_{CN}/Yb_{CN} ratios from 7.3 to 19 and from 17.5 to 49, whereas heavy rare earth elements (HREE) show flat patterns with Gd_{CN}/Yb_{CN} values of 1.5–3.0 and 2.4–5.1 for the Seidorechka Sedimentary and

Umba Sedimentary formations, respectively. Negative Eu anomaly (Eu_{CN}/Eu^*_{CN}) is prominent in samples of both the Seidorechka Sedimentary and Umba Sedimentary formations but there is no Ce anomaly and the Ce_{CN}/Ce^*_{CN} values average at 1.02 ± 0.05.

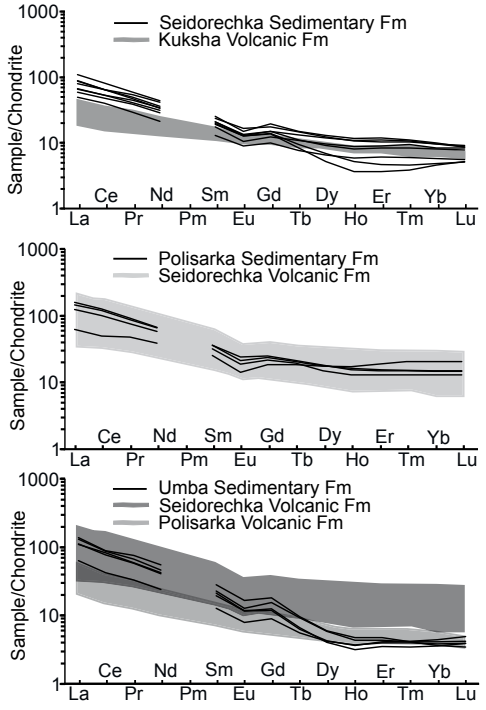

Figure 9. *The chondrite (Taylor and McLennan, 1981) normalized REE patterns. A – Seidorechka Sedimentary Formation (this study) compared with the Kuksha Volcanic Formation (data from Arzamastsev et al., 2020); B – Polisarka Sedimentary Formation (data from Gärtner et al., 2012) and the Seidorechka Volcanic Formation (data from Arzamastsev et al., 2020); C – Umba Sedimentary Formation (this study) compared with the Seidorechka and Polisarka Volcanic formations (data from Arzamastsev et al., 2020). Note the more felsic composition of the Umba Sedimentary Formation compared to the Seidorechka and Polisarka Sedimentary formations that have a mafic composition with a possible signature of Archaean granitized gneisses.*

5. DISCUSSION

5.1. Kuksha palaeoweathering crust

5.1.1. Palaeoclimatic interpretation of the Kuksha palaeoweathering

The thickness of the Kuksha palaeoweathering crust is about 10 m. The uppermost 1.5–2 m part of the crust (interpreted as saprolite) is characterized by the appearance of siderite and dickite, significant element mass-balance enrichment of SiO_2, Fe_2O_3 and P_2O_5 and depletion of MgO and Na_2O. The lower part of the palaeoweathering crust (interpreted as representing saprock) starts at 2 m below the top of the palaeoweathering surface. It extends to ca. 8 m below the top of the palaeoweathering surface where nearly unweathered parent rock commences, marked by the distinct appearance of amphibole.

The correlation between the CIA and CIA – K and the mass-balance calculations of the Kuksha palaeoweathering crust show that the upper 3 m of the weathering profile has suffered from metasomatic potassium overprint (Fedo et al., 1995). This means that the interval now represented by K-rich micas most likely had originally been rich in smectitic and kaolinite clays.

Nevertheless, the high CIA – K values in the uppermost part of the Kuksha basalt in the weathered section reaches values up to 91, suggesting above-average weathering intensity that is further supported by nearly complete weathering of plagioclase and formation of clay/phyllosilicate minerals. Similarly, the mafic index of alteration $MIA_{(R)}$, applicable to mafic rock weathering in reducing environments (Babechuk et al., 2014), shows an increasing trend from values around 25 (unweathered rock) to about 45 that is comparable to strongly weathered Deccan basalts.

Intense weathering and leaching during the formation of the Kuksha palaeoweathering crust is in general agreement with other studies reporting strong weathering at the Archaean–Proterozoic transition (Lowe and Tice, 2007; Young, 2013). Typically, Al-rich clay materials such as kaolinite are formed under intense weathering but kaolinite is not commonly preserved in Palaeoproterozoic and older weathering crusts, being rather replaced either by sericite (Rye and Holland, 2000; Nedachi et al., 2005), illite (Mohanty and Nanda, 2016) or illite-sericite (Teitler et al., 2015). In the Kuksha palaeoweathering profile the kaolinite seems to be replaced by kaolinite polymorph dickite and muscovite-composition mica. The latter can alternatively represent a recrystallized Al-rich smectite. The Fe-rich chlorite in the weathering profile has probably developed at the expense of Fe(II)-rich vermiculite or smectite (Murakami et al., 2004).

Both the indications of intense leaching and formation of kaolinite-type clay minerals in the Kuksha palaeoweathering crust suggest acidic (low-pH) conditions during weathering (Soomer et al., 2019 – PAPER I). Compared to the parent rock, the Kuksha palaeoweathering crust shows an abrupt increase in the Ba/Sr values of ≥10 that are characteristic of weathering in a strongly acidic environment (Retallack, 2001; Sheldon and Tabor, 2009). However, Ba can often be co-

enriched along with K and Rb in metasomatized weathering crusts (Rye and Holland, 2000). Hence the Ba/Sr ratio increase in the Kuksha weathering crust carries a mixed signal of Sr depletion, indicating plagioclase loss during the weathering and Ba-addition following a later K-metasomatism.

Nevertheless, the acidic, low-pH nature of the Kuksha palaeoweathering crust is further indicated by the palaeo-pH proxy AlCa that is based on the acid sensitivity of Ca cations (Lukens et al., 2018). The palaeo-pH values estimated using the AlCa proxy define the parent rock as alkaline with the more intensely weathered upper part where pH varies between 5.0 and 5.5. This model has been previously successfully applied to the Triassic (Lukens et al., 2018) and more recently to the ~600 Ma old Baltic palaeosol (Driese et al., 2018) and the ~1.7 Ga Baraboo palaeosol (Medaris et al., 2017).

In addition, the Cr/Ti ratio showing preferential Cr loss with respect to parent rock in the uppermost 0.5–1 m zone agrees well with the low-pH zone estimates of the AlCa proxy. Chromite is a major carrier of Cr in ultramafic and mafic rocks (Smit and Mezger, 2017) and its solubility is strongly pH-dependent. It becomes dissolved at pH <6 (Oze et al., 2007), in the same range of pH conditions estimated for the 2.50–2.44 Ga Kuksha palaeoweathering crust. Furthermore, Konhauser et al. (2011) demonstrated that Cr has been immobile on land prior to 2.48 Ga, whereas younger geologic samples show extensive leaching of Cr.

The development of weathering crusts is strongly dependent on the climate including mean annual temperatures (MAT) and mean annual precipitation (MAP). However, great caution needs to be taken when using MAT and MAP climofunctions to characterize environmental conditions during the formation of ancient palaeosols. Firstly, because most of the climofunctions employed in palaeosol studies were developed for application to specific soil types and horizons (e.g. Bw or Bt horizons). Thus, these proxies may not be directly applicable to other or unspecified soil types and horizons. Secondly, the geochemistry of the palaeoweathering crust is generally altered by diagenetic and metamorphic processes with the effect increasing with time (Sheldon and Tabor, 2009). For example, the MAT estimation obtained using the salinization model (Sheldon et al., 2002) was specifically developed for soils formed in arid-semiarid settings. This model does not consider the effects of K-metasomatism as apparent in the Kuksha palaeoweathering profile (Soomer et al., 2019 – PAPER I). Similarly, the MAT estimations obtained using the clayeyness model (Sheldon, 2006) have been mainly applied to Quaternary, Miocene and Eocene–Oligocene palaeosols (Sheldon, 2006, 2009; Hamer et al., 2007) and their suitability for Precambrian palaeosols has not been tested.

Despite these shortcomings, many different climofunctions are widely used in palaeosol studies, including Precambrian palaeosols, in order to constrain the climatic conditions during their formation (Retallack, 2008; Sheldon and Tabor, 2009; Driese et al., 2011, 2018; Liivamägi et al., 2015; Medaris et al., 2018; Retallack and Noffke, 2019). Given all these caveats, the estimates that can be provided for Kuksha palaeoweathering should be considered as indicative of palaeoclimate conditions and thus first-order approximations.

Therefore, using the average values of the upper 2.8 m of the Kuksha palaeoweathering profile is not ideal as the PPM1.0, CIA – K and salinization based paleoclimate models for that matter, were designed on the uppermost Bw or Bt horizons geochemistry (Stinchcomb et al., 2016). The "Bw or Bt horizons" method was chosen when building the PPM1.0 because: (1) subsoil horizons are more frequently preserved in the rock record, (2) this subsoil zone reflected weathering without anthropogenic alteration and (3) there were likely less contributions of unaltered parent material sourced from the underlying weathered parent material. However, it is difficult to assess which, if any, horizon in the Kuksha profile is a Bw or Bt horizon.

To overcome the limitation with PPM1.0, we examined two well-studied modern mafic weathering profiles having regolith thicknesses and total Fe contents similar to those in the Kuksha profile (Kim et al., 2017; Stinchcomb et al., 2018). These two weathering profiles have regolith thicknesses of 1.4–3.8 m and modern MAP ranging from 1049 to 1146 mm yr^{-1} and MAT ranging from 11.5 to 12.6 °C. Furthermore, calcite was detected in these otherwise humid weathering profiles (Bazilevskaya et al., 2015) at depth similar to the Kuksha palaeoweathering profile (Somelar et al., 2020 – PAPER II). The best estimates of MAP and MAT for these profiles are higher but similar to modern-day climate estimates. Although only two modern mafic weathering profiles were used, the PPM1.0 results suggest that the mean regolith profile reflects, to a degree, the climate under which it weathered. This provides us with some confidence when using the "regolith averaging" approach, as done for calculating the Kuksha MAP and MAT (Somelar et al., 2020 – PAPER II).

Considering the arguments above, we can suggest that the molecular palaeoclimate indices of the Kuksha palaeoweathering crust show its formation in a cool, temperate climate with mean annual temperatures of ~12.8 ± 4.0 °C according to the PPM1.0 model, ~12.8 ± 4.4 °C by the salinization model and ~12 ± 0.6 °C based on the clayeyness model. Moreover, if in the salinization model K_2O_{CALC} is used instead of measured K_2O, the MAT estimate is the same within ±0.5 °C (Somelar et al., 2020 – PAPER II).

The MAP during the formation of the Kuksha palaeoweathering crust can be estimated between 600 and 1300 mm yr^{-1} (average 1100 mm yr^{-1}) using the CIA – K model and 396 and 1248 mm yr^{-1} (best estimate 784 mm yr^{-1}) by the PPM1.0 model. In addition, the PPM1.0 best estimate is also consistent and within the error of a more recently published random forest model for predicting MAP (Lukens et al., 2019) – the RFMAP2.0 model – that yields average estimates of 740 ± 209 mm (using K_2O) and 679 ± 209 mm (using K_2O_{CALC}) (Somelar et al., 2020 – PAPER II).

These climatic conditions roughly correspond to the modern Mediterranean climate zone at 30–45° latitudes. The Mediterranean climate is characterized by large seasonal contrast in temperature and rainfall (dry summer, cool wet winter). The amount of precipitation falling during winter can be at least three times greater than in summer. The mean annual precipitation varies between 300 and

1500 mm and mean annual temperatures between 11 °C (central Spain) and 19 °C (Cyprus) (Torrent, 2005).

Although Archaean to Palaeoproterozoic palaeogeographic reconstructions of Fennoscandia contain significant uncertainties due to a lack of high-quality palaeomagnetic data and poor dating results (e.g. Buchan, 2014), the palaeomagnetic studies of ~2.45 Ga rocks of the Kola and Karelian provinces support the existence of a single craton and thus the Karelian and Kola cratons can be considered to have the same palaeoposition (e.g. Mertanen and Pesonen, 2005; Mertanen et al., 2006, 2011). Therefore, it is interesting that the predicted palaeoclimatic conditions and expected latitudes are in agreement with the palaeoposition of the craton within southerly palaeolatitudes between 20° and 40° at the beginning of the Proterozoic at 2.5–2.4 Ga (Arestova et al., 2002; Mertanen and Pesonen, 2005; Mertanen et al., 2006; Lubnina et al., 2017).

The Kuksha palaeoweathering crust also shows an enrichment of siderite and depletion of CaO in the upper part of the profile and the accumulation of calcite below 1.5–2 m depth (Soomer et al., 2019 – PAPER I). Although petrographic observations did not show the presence of typical caliche or pedogenic carbonate microstructures, the development of a calcite-rich front at specific depths is suggestive of climate seasonality, which suggests that the Kuksha palaeoweathering crust formed under semi-arid climate agreeing with the climatic conditions based on climofunction estimates.

Moreover, compared to other Archaean–Proterozoic weathering crusts/ regoliths described in Fennoscandia, the Kuksha palaeoweathering crust shows higher weathering intensity. Laajoki et al. (1989) and Sturt et al. (1994) have ascribed the formation of these regoliths to physical *in situ* weathering under an arid to semi-arid palaeoclimate. Nearly all weathering crusts at the base of the Palaeoproterozoic sedimentary-volcanic units in Fennoscandia are characterized by high abundance of carbonate, particularly in the uppermost zone of the weathering crust and in the conglomerate units. According to Kirsimäe and Melezhik (2013), this indicates a caliche-type soil (Aridisol) evolution in arid or semi-arid climate, where evaporation caused alkali supersaturation in soil solution.

Most modern calcic soils typically form at low latitudes in arid and semi-arid climates where MAP is less than 800 mm yr^{-1}, with some exceptions 800–1000 mm yr^{-1} (Mack and James, 1994). These soils are also formed where there is seasonal difference in temperatures, e.g. hot summers and warm winters at low latitudes and hot summers and cool winters at higher latitudes (Mack and James, 1994). Additionally, pedogenic carbonates characteristic of calcic soils typically form in well-drained soils of sub-humid, semi-arid and arid climate (Srivastava et al., 2002), whereas in poorly drained/waterlogged anoxic soil environments pedogenic siderite (also characteristic of Kuksha palaeosol) is more common (Ludvigson et al., 1998).

5.1.2. pO_2 and pCO_2 estimation from the composition of the Kuksha palaeoweathering crust

The formation of secondary mineral assemblages in weathering processes is strongly defined by the oxidation state of the atmosphere, water–rock ratio and pCO_2. Typically, the most mobile elements in the Kuksha palaeoweathering crust, such as the alkali- and alkaline-earth elements, were removed from basaltic parent rock consisting of pyroxene, olivine, amphibole and feldspars (Nesbitt et al., 1980). Interestingly, the upper part of the crust shows an apparent enrichment of Fe (τ values of 25–30%). Unlike the alkali- and alkaline-earth elements, Fe is redox-dependent during weathering. Reducing environments mobilize Fe^{2+} and, normally, it is leached out along with Mg, but under oxidative conditions insoluble Fe^{3+} is formed and accumulated together with Al (Babechuk et al., 2014). The Fe-enrichment in the Kuksha palaeoweathering crust is rather not connected with oxidative conditions but results from rock leaching and Fe reprecipitation as siderite in the upper 2 m of the preserved profile (Soomer et al., 2019 – PAPER II). Therefore, following Rye and Holland (2000) and Ohmoto et al. (2004), it can be suggested from the relative abundance of siderite together with the kaolin group mineral dickite, traces of pyrite and the absence of Fe-oxide/oxyhydroxides in the upper part of the studied palaeoweathering section that the Kuksha weathering crust formed in the absence of oxygen and under high partial CO_2 pressures (above 0.1 atm) (Soomer et al., 2019 – PAPER I).

Indeed, anoxic conditions are also indicated by the presence of the mineral rhabdophane [(La, Ce, Nd)$PO_4 \cdot nH_2O$] in the upper layers of the Kuksha palaeoweathering crust. Rhabdophane forms during the weathering process only when reduced Ce(III), along with tri-valent La(III) and Pr(III), is available and Ce is not oxidized into Ce(IV). The mineral is resistant to metamorphism (Banfield, 1989; Murakami et al., 2001), thus providing even more confidence in the interpretation of anoxic conditions. In addition, redox-sensitive element ratios, such as V/Al and V/Ti, have constant values throughout the Kuksha palaeoweathering crust, which shows that V was not leached and the environmental conditions could have been anoxic at the time of weathering (Rye and Holland, 2000).

Ohmoto et al. (2004) have suggested that siderite formation indicates specific environmental conditions with the very low $pO_2 << 0.1$ PAL, extremely high $pCO_2 > 100$ PAL, slightly acidic to neutral pH (5.5–7.5) and high concentration of Fe^{2+}. However, other studies have noted that siderite alone does not necessarily indicate either the presence of low pO_2 or high pCO_2 atmospheric conditions as siderite is common in modern soils forming in poorly drained/waterlogged anoxic environments (Ludvigson et al., 1998). Hao et al. (2017) recently showed that the redox states of Archaean surface environments were controlled by H_2 instead of very low O_2, and pyrite and siderite are thermodynamically stable phases relative to hematite over a wide range of pCO_2 (1 to >500 PAL) regardless of kinetic effects. Additionally, using laboratory experiments to explain siderite formation in sedimentary Banded Iron formations (BIF) of the Archaean–Proterozoic, Gäb et al. (2017) suggested that siderite precipitation is not achieved at any specific

levels of pCO_2, thus questioning the use of sedimentary siderite as an indicator of palaeoatmosphere CO_2 levels. Instead, they suggested that bacterial influence is needed for siderite to form (e.g. Sawicki, 1995; Kholodov and Butuzova, 2008). Driese et al. (2010) drew the same conclusion for historical (<100 yr old) pedogenic siderite formed in association with accelerated bacterial degradation of anthropogenic creosote and coal tar deposits. Therefore, siderite precipitation requires neither extremely high CO_2 nor low O_2 levels and its presence alone cannot be used as a clear indicator of high pCO_2 and low pO_2 environments.

Nevertheless, palaeoatmospheric CO_2 levels can be estimated using a Precambrian palaeosol palaeobarometer developed by Sheldon (2006). It is based on the total mass flux of non-carbonate CaO, MgO, Na_2O and K_2O_{CALC} in the weathering profile as a function of time and weathering conditions like duration, rainfall rate and weathering depth. Assuming the maximum timeframe for the weathering of the Kuksha palaeoweathering crust of ca. 60 My (Soomer et al., 2019 – PAPER I), the estimates for palaeoatmospheric pCO_2 suggest values between 1.7 and 20 times PAL (Somelar et al., 2020 – PAPER II). Mean annual precipitation estimates for the Kuksha palaeoweathering crust based on CIA – K are in the range of 800–1000 mm yr^{-1}, and the best estimates of MAP using PPM1.0 (and upper 2.71 m of the regolith) are 763 and 783 mm yr^{-1}, whereas the latter value was obtained from geochemical assays that use K_2O_{CALC}. The depth of the groundwater table could be placed at ca. 2 m according to changes in weathering intensity (CIA – K values) and carbonate accumulation.

The best guess for the pCO_2 levels of the Kuksha palaeoweathering crust would be between 2 and 10 times PAL, whereas the greater depth of the groundwater level, e.g. at 4 m, would increase the pCO_2 PAL estimate by a factor of two and *vice versa* if the groundwater level was lower but the magnitude was in the same range (Figure 10).

A similar range of the palaeoatmospheric pCO_2 estimates is achieved using the carbonate isotope-based CO_2 palaeobarometer (Cerling, 1984; Ekart et al., 1999) with the siderite $\delta^{13}C$ composition suggesting values of 0.1 and 4 PAL, while pCO_2 estimates using $\delta^{13}C$ of calcite suggest values of 1.2–8.5 PAL (Somelar et al., 2020 – PAPER II). These estimates are in good accordance with the pCO_2 estimates using the mass-balance model though the pedogenic carbonate model was developed on the basis of modern soil carbonate dynamics in arid and semiarid climates where calcium carbonate precipitates in soil are common (Royer 1999, 2014). Also, this model has not been used extensively in palaeosols older than Early Silurian, when supposedly modern soil carbon dynamics evolved (Cotton and Sheldon, 2012). On the other hand, the primitive nature of dry, vegetation-poor Aridisols would resemble the Precambrian palaeosols the most, as these are believed to have had primitive ecosystems with low bioproductivity, and that during carbonate formation the soil-respired CO_2 was mixed with the atmospheric CO_2 in the open system (Sheldon and Tabor, 2009).

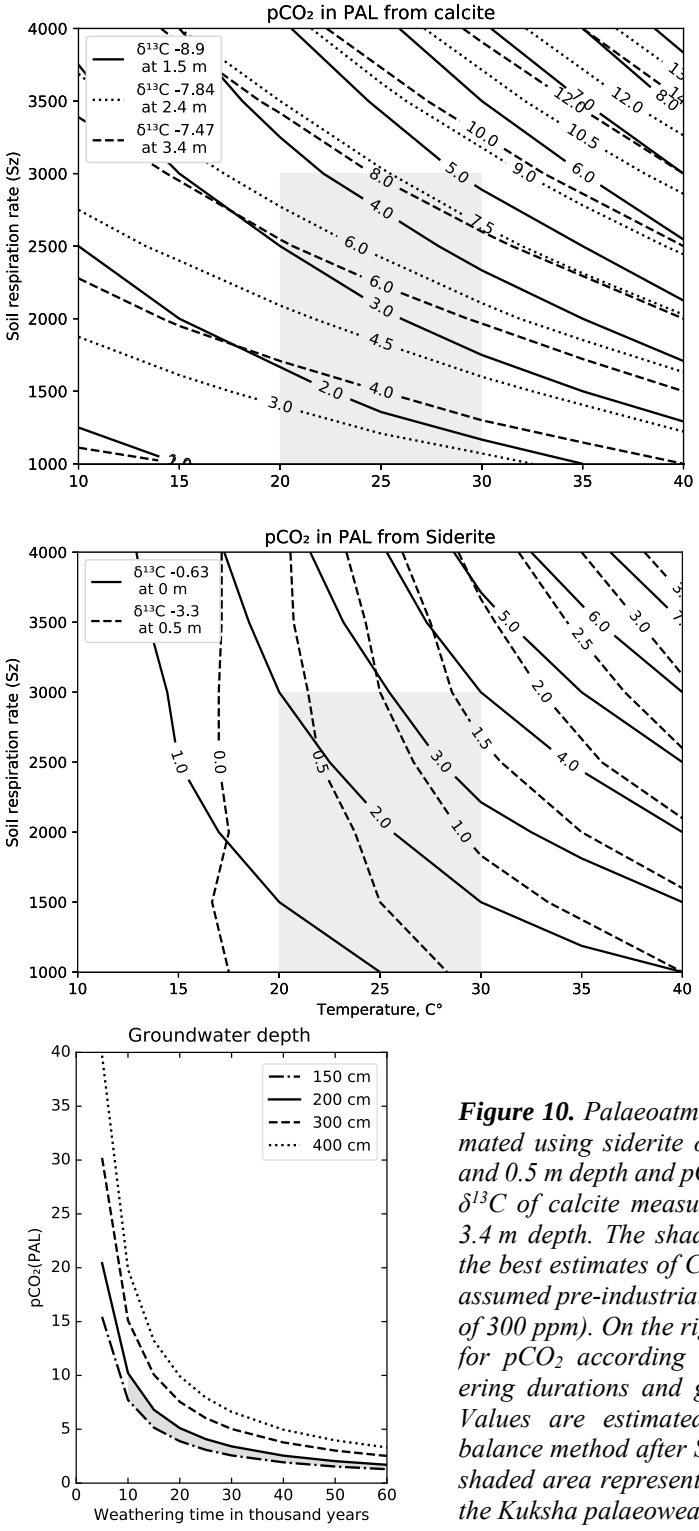

Figure 10. *Palaeoatmospheric pCO_2 estimated using siderite $\delta^{13}C$ measured at 0 and 0.5 m depth and pCO_2 estimated using $\delta^{13}C$ of calcite measured at 1.5, 2.4 and 3.4 m depth. The shaded area represents the best estimates of CO_2 levels (based on assumed pre-industrial modern CO_2 levels of 300 ppm). On the right modelled values for pCO_2 according to different weathering durations and groundwater levels. Values are estimated using the mass-balance method after Sheldon (2006). The shaded area represents the best guess for the Kuksha palaeoweathering crust.*

The oldest palaeosols containing pedogenic carbonate nodules that are known to have been formed *in situ* are as old as 2.6 Ga, and geochemical evidence dates the first terrestrial ecosystems also back as early as 2.6 Ga (Watanabe et al., 2000). Homann et al. (2018) have shown that conglomerates and sandstones of the 3.22 Ga Moodies Group, South Africa, contain putative fossilized terrestrial microbial mats with average $\delta^{13}C$ values of organic matter around –21.2‰.

Although based on different algorithms, both methods lead to the best pCO_2 estimates in the same range between 1 and 10 times PAL. Therefore, the estimate for the 2.44–2.5 Ga Kuksha palaeoweathering crust is somewhat lower but in general agreement with some recent atmosphere models, however, at least an order of magnitude less than 160–490 PAL obtained by Kanzaki and Murakami (2015, 2018b) for ~2.46 Ga (Figure 11). Previously, Sheldon (2006) and Mitchell and Sheldon (2010) have suggested CO_2 levels being below 20 PAL at 2.5–1.8 Ga and dropping to 4–6 PAL between 1.8 and 1 Ga. Driese et al. (2011) calculated pCO_2 levels at ca. 41 PAL in the 2.69 Ga Saganaga tonalite palaeosol. Medaris et al. (2017) estimated the pCO_2 level at ca. 5 PAL in the 1.7 Ga Baraboo palaeosol. Very low pCO_2 levels of 2.1 ± 0.5 PAL were reported for a 3.7 Ga palaeosol in the Isua Greenstone Belt by Retallack and Noffke (2019). Similarly, Alfimova et al. (2014) suggest that the pCO_2 levels of the Neoarchaean and Palaeoproterozoic were rather similar to those of the Phanerozoic, most likely not much over 25 PAL. In contrast, Kanzaki and Murakami (2015) give CO_2 levels between 85 and 510 PAL for most of the Archaean and ca. 160–490 PAL in the early Palaeoproterozoic at ca. 2.46 Ga, whereas Ohmoto et al. (2004, 2014) have urged that the pCO_2 levels before ~1.8 Ga had to have been well over 100 times PAL. The Kanzaki and Murakami (2015, 2018b) model applies balanced calculation between rock and water phases, charge balance in porewater and thermodynamics of the weathering secondary minerals, and tends to overestimate the pCO_2 level estimates based on mass-balance models (e.g. Sheldon, 2006). Interestingly, in the Kuksha case the two models (mass-balance vs. carbonate isotope composition) based on different principal assumptions give similarly low pCO_2 estimates.

If the palaeoatmospheric CO_2 levels of <10 PAL during the formation of the Kuksha palaeoweathering crust is considered in a global context, it should be noted that this crust was developed at the time of the breakup of the Kenorland (Superia) supercontinent dated at ca. 2.45 Ga (Ojakangas et al., 2001). It predates the GOE at ca. 2.43 Ga (Gumsley et al., 2017) but coincides with the onset of a series of large-scale Huronian glaciations (Young, 2019). Most likely, at that time, the widespread production of basalts caused increased CO_2 inputs into the atmosphere, which, in turn, were balanced by the emergence of continental cratons above sea level and continental weathering causing drawdown of atmospheric CO_2 that led to a reduced greenhouse effect. This process, in and of itself, could have initiated glaciations that might have reached the snowball Earth state (e.g. Kirschvink et al., 2000; Kopp et al., 2005; Hoffman et al., 2017). In this context it is also important to mention that sulphur isotopes of sulphides in the Seidorechka Sedimentary Formation just above the Kuksha palaeoweathering crust show a weak mass-independent fractionation (MIF) signal (Warke et al. 2020) that further supports the oxygen-depleted conditions during the Kuksha palaeosol

formation. However, if the MIF signal generally means that the pO_2 level was not higher than 10^{-5} times PAL (Bekker et al., 2004), the weakened MIF signal in the Seidorechka Sedimentary Formation could point, in this case, to the initiation of planetary oxygenation or enhanced glacial activity, as was suggested for Huronian glaciogenic sediments in the Transvaal and Huronian Supergroups (Kopp et al., 2005).

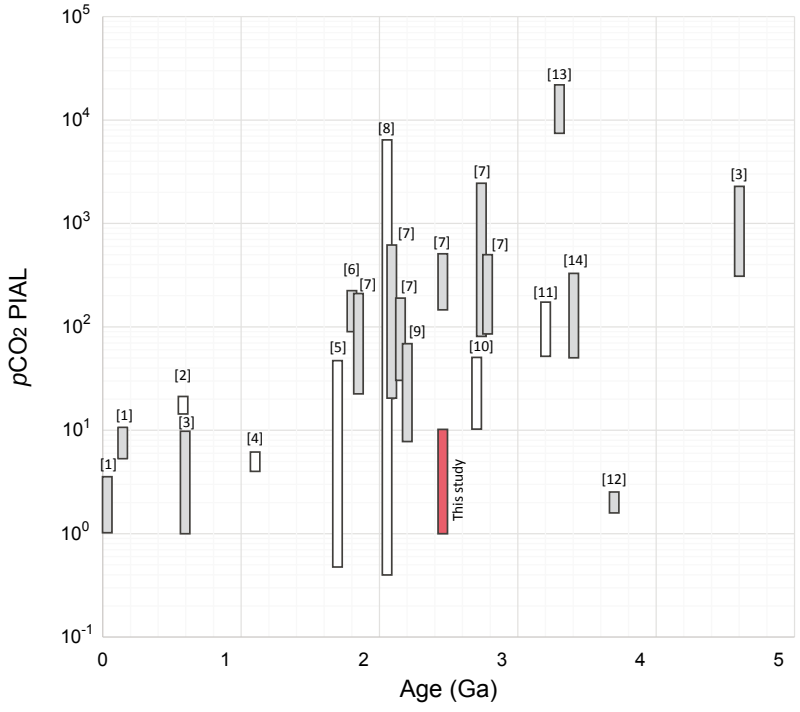

Figure 11. *Calculated pCO_2 values over the history of the Earth. The pCO_2 estimations from the Kuksha palaeoweathering crust are marked with red, and other estimates made using the Sheldon (2006) mass-balance approach are denoted in white colour. The grey colour represents other palaeosol-based model estimates obtained using reaction-products and/or palaeosol mineralogy. Estimates are from: 1, Cerling (1992); 2, Driese et al. (2018); 3, Kasting (1993); 4, Mitchell and Sheldon (2010); 5, Medaris et al. (2017); 6, Ohmoto et al. (2004); 7, Kanzaki and Murakami (2015); 8, Rybacki et al. (2016); 9, Sheldon (2006); 10, Driese et al. (2011); 11, Hessler et al. (2004); 12, Retallack and Noffke (2019); 13, Rosing et al. (2010); 14, Lowe and Tice (2004)*

The Huronian-age glaciogenic sediments in the Imandra–Varzuga Greenstone Belt are known from the Polisarka Formation above the Seidorechka Volcanic Formation overlying the Kuksha Formation (Melezhik et al., 2013). The depositional age of the Polisarka Sedimentary Formation is constrained to 2434 ± 6.6 Ma, derived from andesitic tuff (Brasier et al., 2013). The Kuksha palaeoweathering crust, with its low pCO_2 level estimates, can thus represent a period of declining CO_2 concentrations leading to the onset of cooling and initiation of Huronian glaciation(s), and also correspond to a time when O_2 levels started to make a change in the Earth's redox system.

5.2. Provenance and weathering intensity at the transition to oxygenated surface environments as recorded from the Imandra–Varzuga Greenstone Belt metasediments

5.2.1. Tectonic setting and provenance

The Imandra–Varzuga Greenstone Belt is the eastern part of the North Transfennoscandian Greenstone Belt (Melezhik and Fallick, 1996). It contains sedimentary units recording the disappearance of the sulphur isotope MIF signal in the lower part of stratigraphy and the LJE carbonate carbon isotope signal in the upper part (Warke et al., 2020), revealing thus the transition from anoxic to oxic atmospheric conditions.

The interpretation of the geotectonic settings (see Figures 9–12 in Soomer et al., 2022 – PAPER III) using different discrimination diagrams like La/Sc vs. Ti/Zr relationships suggests predominantly oceanic island to continental island arc setting for the Seidorechka Sedimentary and Polisarka Sedimentary formations and a change towards a passive continental margin during the deposition of the Umba Sedimentary Formation. A similar conclusion can be drawn from the Sc–Th–Zr/10, Th–La–Sc and Co–Th–Zr/10 relationships where the Seidorechka and Polisarka formation sediments show a predominantly oceanic island arc setting and the sediments of the Umba Sedimentary Formation sediments formed in a continental island arc setting. However, the discrimination plots distinguishing between the collision-convergent, island or continental arc, and continental rift tectonic zones by Verma and Amstrong-Altrin (2013) show that the low silica samples (35–63 wt% SiO_2), represented mainly by the Seidorechka and Polisarka Sedimentary formations, range from island or continental arc settings to the continental rift to collision-convergent tectonic setting. Most of the high silica samples of the Umba Sedimentary Formation (63–95 wt% SiO_2) plot in the continental rift field close to the junction point with the island-continental arc and collision-convergent tectonic setting fields (Figure 11 in Soomer et al., 2022 – PAPER III).

The interpretation of the Umba Sedimentary Formation tectonic setting related to the continental rifting agrees well with the general geotectonic model (Melezhik and Sturt, 1994; Melezhik and Hanski, 2013). The development of the Pechenga and Imandra–Varzuga Greenstone belts was initiated as an intracontinental rift structure at ca. 2500–2400 Ma in association with the break-up of the Archaean supercontinent (Skyttä et al., 2019), and reached a major stage of inversion prior to renewed rifting and deposition that started at ca. 2390 Ma. Melezhik and Sturt (1994) suggested that the Pechenga and Imandra–Varzuga Belts developed from the Afar Triangle–East African type rifting during the deposition of the Seidorechka Sedimentary and Polisarka Sedimentary formations (ca. >2500–2100 Ma) to the Red Sea type rifting during the formation of the Umba Sedimentary Formation (2100–1970 Ma), and the system was finally commenced by a possible oceanic spreading phase at 1990–1970 Ma.

The shale, shale-siltstone and greywacke lithologies in all formations have Al_2O_3/TiO_2 ratio values reaching >20, suggesting provenance from mixed felsic to intermediate rocks (Hayashi et al., 1997), with a few samples indicating an intermediate and mafic source. However, in the provenance rock discrimination diagram of Roser and Korsch (1988) most of the Seidorechka Sedimentary Formation samples are in the field of mafic igneous rocks and some samples (also samples of the Polisarka Sedimentary Formation) plot close to or in the intermediate igneous rocks field (Figure 12b in Soomer et al., 2022 – PAPER III). The Umba Sedimentary Formation shales and shale-siltstones plot mostly in the fields of felsic and quartzose provenance, whereas the quartzose recycled sedimentary field represents quartzitic or weathered granitic-gneiss terrain or a recycled sedimentary source with loss of feldspars and increase in quartz content (Mattos and Batezelli, 2019).

The strong felsic provenance signature of the Umba Sedimentary Formation is further supported by LREE enrichment (higher La_{CN}/Yb_{CN} ratios) and flatter HREE segments compared to those of the Seidorechka Sedimentary Formation (see Figure 7 in Soomer et al., 2022 – PAPER III). In addition, the distinctly different provenance of the Seidorechka and Polisarka, and Umba formations is clearly evident from the nearly consistently positive sediment protolith ψ values (Figure 12; Lipp et al., 2020) of the Umba Sedimentary Formation indicating a more felsic source compared to the modern Upper Continental Crust (UCC), whereas the Seidorechka Sedimentary Formation samples and most samples of the Polisarka Sedimentary Formation show negative ψ values indicative of mafic protolith (Lipp et al., 2020).

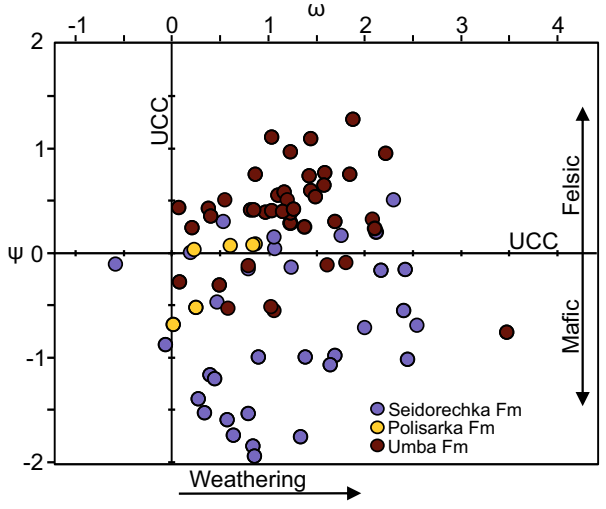

Figure 12. *Weathering intensity and provenance variation in the studied siliciclastic samples after Lipp et al. (2020) indicating a more felsic composition for the Umba Formation compared to the Seidorechka and Polisarka Formations.*

Similarly, the TiO_2 vs. Zr plot (see Figure 12c in Soomer et al., 2022 – PAPER III; Hayashi et al., 1997) suggests the intermediate igneous rocks provenance for the Seidorechka Sedimentary and Polisarka Sedimentary formations and shows that most of the Umba Sedimentary Formation sediments fall in the felsic igneous rock field with strong Zr addition. Sediment recycling and clear Zr addition in most of the Umba Sedimentary Formation samples is evident from the Th/Sc vs. Zr/Sc plot (see Figure 8 in Soomer et al., 2022 – PAPER III). All samples from the Seidorechka Sedimentary and Polisarka Sedimentary formations and only some samples of the Umba Sedimentary Formation plot close to the crustal compositional variation and suggest a limited recycling and/or sedimentary sorting, but the pronounced Zr enrichment of the Umba Sedimentary Formation is likely caused by sediment recycling due to several erosion-transport-deposition cycles. The uplift and deep erosion at the boundary between the Seidorechka and Polisarka–Umba Sedimentary formations marked by an erosional contact with widespread regolith-type weathering crusts in the Pechenga and Imandra–Varzuga Greenstone belts in eastern Finland and Karelia, including the Onega Basin (Sturt et al., 1994; Laajoki, 2005; Kirsimäe and Melezhik, 2013), is dated between 2396 and 2330 Ma (Melzhik et al., 1994). The Polisarka Sedimentary Formation, characterized by mafic-intermediate sediment protolith signatures, lies unconformably on the Seidorechka Volcanic Formation. The basal conglomerate of the Polisarka Sedimentary Formation contains variably weathered clasts of dacites, andesites and basaltic andesites from the Seidorechka volcanic rocks (Melezhik et al., 1982), suggesting together with geochemical signatures that the Polisarka sediments mainly originate from the weathering and erosion of the Seidorechka Volcanic Formation. This is further signified by detrital zircon U–Pb ages in the Polisarka Sedimentary Formation diamictite (Gärtner et al, 2014) showing a bi-modal distribution with maxima at ca. 2450 Ma corresponding to the age of the Seidorechka Volcanic Formation at ca. 2441 Ma (Amelin et al., 1995) and the pronounced zircon population with 2600–2900 Ma ages. The last population indicates an input from the weathering of the siliciclastic rocks in the surrounding Archaean provinces (Kola and Karelian Province and Murmansk Craton). This population is also the dominant detrital zircon age group in the Seidorechka Sedimentary Formation with an average at ca. 2750 Ma (Gärtner et al., 2014; Smolkin et al., 2020). Other detrital zircon age groups in the Seidorechka Sedimentary Formation are at ca. 2850 Ma, and a younger subordinate group between 2450 and 2500 Ma, possibly indicating the material eroded from the underlying Kuksha volcanic rocks.

The Umba Sedimentary Formation that rests with a depositional contact on volcanic rocks of the Polisarka Volcanic Formation (Melezhik et al., 2013) bears a geochemically different signal and it has been suggested as derived from the erosion of the Seidorechka volcanic rocks (Bekasova and Pushkin, 1977). While the lower part of the nearly 3000-m-thick Seidorechka Volcanic Formation (Melezhik and Strut, 1994; Chashchin et al., 2008; Hanski, 2013; Arzamastsev et al., 2020) is composed of komatiitic basalts, basaltic and basaltic andesite flows interbedded with gabbroic and pyroxenitic sills succeeded by subaerial

amygdaloidal komatiitic basalts, basaltic andesites and andesites, the upper part of the succession is represented by more felsic volcanics – dacites, dacitic rhyolites and rhyolites intruded by the Imandra layered gabbro-norite lopolith (Chashchin et al., 2008; Hanski, 2013; Arzamastsev et al., 2020). The uplift and erosion of these felsic units, possibly mixed with erosion weathered Archaean granitized gneisses of the Kola Province, served as a provenance for the Umba Sedimentary Formation. This is apparent from REE distributions in the Umba Sedimentary Formation showing increased LREE, a steep declining trend to low HREE contents and only moderate negative Eu anomalies (see Figure 7 in Soomer et al., 2022 – PAPER III).

The geochemistry of the Seidorechka, Polisarka and Umba Sedimentary formations shows that the uppermost Umba Sedimentary Formation bears a felsic (dacitic) signature and is compositionally different from the Seidorechka and Polisarka Sedimentary formations that exhibit a more mafic/andesitic signature with significant input from Archaean metamorphic terranes (Soomer et al., 2022 – PAPER III).

5.2.2. Weathering intensity

The weathering trend of a given igneous protolith should be subparallel to the A–CN axis in the A–CN–K plot (Figure 13) (Nesbitt and Young, 1984). Different diagenetic and metamorphic effects, particularly the K-metasomatism, can cause an offset from the theoretical weathering trend towards the K_2O apex (Fedo et al., 1995; Tosca et al., 2010; Bahlburg and Dobrzinski, 2011). The K-metasomatism is governed either by illitization (K-uptake) of smectitic clay minerals (and kaolinite) forming during the moderate-to-intensive weathering, or by plagioclase replacement by K-feldspar. However, while the former causes a shift to seemingly lower weathering intensity (e.g. leads to lower CIA values), the latter does not affect weathering intensity estimate because of the mole-for-mole substitution of K for Ca/Na (Bahlburg and Dobrzinsk, 2011).

The A–CN–K ternary plot of the Seidorechka, Polisarka and Umba Sedimentary formations shales displays a linear weathering trend (Figure 13) typical of sediments affected by K-metasomatism. The Seidorechka Sedimentary Formation shales show the least inclined trend from the A–CN line and is farther away from the K_2O apex compared to shales of the Polisarka and Umba Sedimentary formations indicating a lower effect of K-metasomatism (Fedo et al., 1995; Bahlburg and Dobrzinsk, 2011).

The downward extension of the weathering trend line of the Seidorechka Sedimentary Formation shales intersects with the Lower Continental Crust (LCC) and/or mid-ocean ridge basalt (MORB) composition supporting the interpretation of mafic/intermediate provenance. Shales of the Umba Sedimentary and Polisarka Sedimentary formations show, however, a significant K-addition and the trend line is significantly biased towards the K_2O apex, whereas the intercept of the trend is in agreement with sediment provenance of the upper continental crust composition.

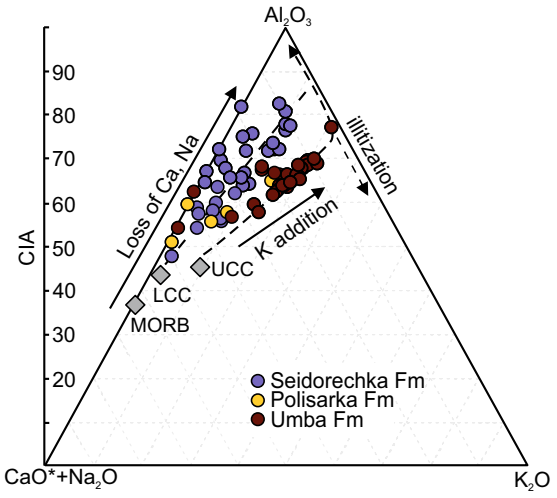

Figure 13. *A–CN–K ternary plot showing weathering trends and overall CIA values, and compositional difference in the weathering protolith among the studied samples. Values for the UCC are from Rudnick and Gao (2014), LCC from Rudnick and Fountain (1995) and MORB from Gale et al. (2013).*

The CIA values of 50–60 indicate low intensity of chemical weathering, while values of 60–80 denote intermediate and those >80 extreme weathering (Nesbitt and Young, 1984; Fedo et al., 1995). The weathering indices (CIA, $CIA_{(K)}$, WIP and $WIP_{(K)}$) of shale and shale-siltstone lithologies show on average intermediate weathering intensity in all formations with CIA values from 52 to 80 (average 66) in the Seidorechka Sedimentary Formation, from 49 to 63 in the Polisarka Sedimentary Formation and from 47 to 75 in the Umba Sedimentary Formation (see Fig. 15 in Soomer et al., 2022 – PAPER III). Correction for K-addition shifts the index $CIA_{(K)}$ to higher values but the weathering intensity still remains at a moderate level. Moderate weathering is also indicated by the average $WIP_{(K)}$ values: 47 in the Seidorechka Sedimentary Formation, 61 in the Polisarka Sedimentary Formation and 48 in the Umba Sedimentary Formation.

Similar to the CIA, $CIA_{(K)}$ and WIP, the average weathering coefficient ω suggests moderate, and in only few samples intense silicate weathering with ω values varying around 1.09 ± 0.84, 0.40 ± 0.36 and 1.18 ± 0.68 in the Seidorechka, Polisarka and Umba Sedimentary formations, respectively (Figure 12; Lipp et al., 2020, 2021). The weathering function ω value of the UCC is at 0; ω values 0–1 indicate low weathering intensity, values 1–3 intermediate intensity and values >3 would suggest intensive silicate weathering (corresponding CIA >80).

Surprisingly, the Seidorechka and Umba Sedimentary formations that deposited before and after the GOE, respectively, show a similar moderate weathering intensity (average $CIA_{(K)}$ values 68), suggesting that (seemingly) there is no significant effect from the onset of oxidative weathering on the overall weathering intensity in the Palaeoproterozoic. However, it should be taken into account that

the intensity of chemical silicate weathering is highly sensitive to source rock lithology, topography, climatic regime – precipitation and particularly to the temperature (Marshall et al., 1988; Wilson, 2004; Hayes et al., 2020) and the atmospheric CO_2 levels (Kump et al., 2000; Dessert et al., 2003; Beaulieu et al., 2012; Winnick and Maher, 2018).

The provenance indicators of the source rocks of the Seidorechka Sedimentary Formation point to a mafic protolith that is by far more susceptible to weathering (e.g. Meunier et al., 2007) than the predominantly felsic protolith of the Umba Sedimentary Formation. Assuming a comparable duration of weathering, the similar weathering indices in both formations advocate a higher weathering intensity in the latter. Moreover, the climatic conditions during the deposition of the Seidorechka and Umba Sedimentary formations, deposited ca. 100–200 Ma apart, might have been considerably different. Li and Yang (2010) reviewed the variation in the weathering intensity indicator (CIA) in modern global drainage basins and concluded that the global integrated weathering history is most sensitive to land surface temperature, latitude at the river mouth and soil depth in drainage basins, whereas the correlation to precipitation, runoff and elevation was insignificant in most basins.

The soil depth drained on continents during the Palaeoproterozoic is difficult to estimate. However, Somelar et al. (2020 – PAPER II) have suggested, from the molecular palaeoclimate indices of the Kuksha palaeoweathering crust which developed right at the base of the Seidorechka Sedimentary Formation, that the weathering occurred in a cool-temperate (possibly Mediterranean-type) climate with mean annual temperatures ca. 12–13 °C and mean annual precipitation 600–1300 mm yr^{-1}. This estimate is in agreement with the palaeoposition of the Kola-Karelia craton within southerly palaeolatitudes between 20° and 30° at the beginning of the Proterozoic at 2.5–2.4 Ga (Arestova et al., 2002; Mertanen and Pesonen, 2005; Mertanen et al., 2006; Lubnina and Slabunov, 2017). The palaeoposition of the Kola–Karelia craton is poorly constrained at the time of the deposition of the Umba Sedimentary Formation between 2306 and 2056 Ma. However, according to Lubnina et al. (2017), the craton was located at ca. 40° to 45° latitudes or even higher by 1975 Ma. If their estimate is correct, the slightly elevated weathering intensity, as recorded from the Umba Sedimentary Formation, was attained at higher latitudes and consequently at lower mean annual temperatures compared to the Seidorechka Sedimentary Formation showing somewhat higher weathering intensity in oxygenated conditions in post-GOE time.

The oxygenation of the atmosphere resulted in significant changes in the weathering chemistry (Hazen et al., 2008; Bahlburg and Dobrzinski, 2011). The first, and most important effect was the change in the behaviour of redox-sensitive elements (Fe, V, U, Mo, S, etc.; Hao et al., 2017) which possibly further amplified the sulphuric acidic attack caused by (bacterially mediated) oxidation of sulphide minerals and siderite present in surface rocks prior to the GOE (Holland, 2006; Konhauser et al., 2011; Bachan and Kump, 2015). As an evidence, the Cr-enrichment in Palaeoproterozoic marine iron formations (Konhauser et al., 2011) has been suggested, being caused by the acidic (pH <4) leaching of Cr from

continental weathering crusts. Also, the distribution of intensely weathered palaeosol profiles in the post-GOE Palaeoproterozoic (Hao et al., 2021) could indicate the intensified acidic continental weathering and leaching following the GOE. Intensive weathering possibly played a critical role in promoting supply of essential nutrients for boosting the bioproductivity that further contributed to the rise of the oxygen levels following the GOE (Mills et al., 2014; Laakso and Schrag, 2018; Crockford et al., 2019; Reinhard et al., 2020).

The weathering intensity is also controlled by concentration changes in atmospheric CO_2 through the influence on the acidity of precipitation and more importantly, by the Earth's surface temperatures over geological timescale (Mills et al., 2019). Feedbacks between the Earth's surface temperature and long-term carbon cycle in response to atmospheric CO_2 levels operate typically over timescales of >100 kyrs (Kasting, 1987). The high weathering intensity (CIA – K values of >90) and development of Al-rich phyllosilicate in the uppermost part of the ca. 2504–2442 Ma Kuksha palaeosol (Soomer et al., 2019 – PAPER I), and also in other palaeoweathering crusts predating the GOE such as the 2760 Ma Mt. Roe palaeosol (Teitler et al., 2015), most likely indicate the intensified weathering due to more acidic rain- and river water (Hao et al., 2017).

As discussed above in the context of Kuksha palaeoweathering, the palaeo pCO_2 estimates for the GOE vary largely from over 400 PAL (Kanzaki and Murakami, 2015) to 41 PAL (Driese et al., 2011) and to even as low as 1–10 PAL recorded in the Kuksha palaeosol (Somelar et al., 2020 – PAPER II). Reasonably, the last low values can be interpreted as resulting from the CO_2 drawdown prior to the onset of the Huronian glaciation (Young, 2019). Further, this low pCO_2 estimate agrees with mass-balance modelling studies of Sheldon (2006), Mitchell and Sheldon (2010) and Medaris et al. (2017), suggesting that CO_2 levels dropped below 20 PAL between 2.5 and 1.8 Ga and were only 4–6 PAL between 1.8 and 1 Ga. A direct consequence of lower pCO_2 at the Archaean–Proterozoic transition could be a progressively lower silicate weathering rate.

Given the decreasing atmospheric pCO_2 levels from the Archaean to the Proterozoic–Phanerozoic, the chemical weathering intensity should have gradually decreased over the time accordingly. Indeed, several earlier studies (Condie, 2001; González-Álvarez and Kerrich, 2012) have demonstrated a steady secular decrease in the CIA values in shales from an average of ca. 80 during the Archaean (80–100 in the Mesoarchaean and 80–90 in the Neoarchaean), ca. 75 in the Proterozoic (70–85) and ca. 70 for average Phanerozoic shales. This controversy of significantly declining weathering intensity towards modern has also been observed in glacial deposits (Li et al., 2016), where a similar secular trend in fine fractions of glacial diamictites is apparent with CIA values decreasing from 80 for the Archaean, 72 for the Proterozoic (74 in the Palaeoproterozoic, 74 in the Mesoproterozoic and 68 in the Neoproterozoic) to only 66 in the Phanerozoic (Cenozoic) diamictites.

Nevertheless, the drastically lower weathering intensity in Cenozoic glacial diamictites has been interpreted to reflect the removal of any weathered regolith by preceding glacial events rather than changing weathering intensity (Li et al.,

2016). A similar reasoning could be applied to the Umba Sedimentary Formation sediments post-dating the global Huronian glaciacion(s) and lacking clear evidence of enhanced weathering in post-GOE oxygenated environments. More intriguingly, on the basis of thermochemical modelling, Fabre et al. (2021) recently concluded that the weathering intensity over the Palaeoproterozoic era was related to the combination of the yet elevated pCO_2 and low pO_2 and was two orders of magnitude greater than tropical present-day weathering intensity. However, they suggest that, apart from the punctuated sulphuric acid intensification effect on the weathering in the oxygenated atmosphere, the long-term influence of the atmosphere oxygenation would have been the opposite as oxygen controls the precipitation of iron oxyhydroxide coatings on weathered minerals, which could have inhibited their further dissolution (Fabre et al., 2021) causing a decrease in overall silicate weathering intensity in Palaeoproterozoic times following the GOE.

6. CONCLUSIONS

The palaeoweathering crust developed on top of the basalts of the Kuksha Volcanic Formation in the Palaeoproterozoic Imandra–Varzuga Greenstone Belt, north-western Russia, ca. 2.44–2.50 Ga ago, predates the Great Oxygenation Event. The most intensely weathered section extends about 1.5–2 m below the palaeoweathered surface and is characterized by high values of CIA – K and $MIA_{(R)}$ – K, suggesting an above-average intensity of weathering. Intense weathering is also supported by the nearly complete weathering of plagioclase and the formation of Al-rich clay minerals in the uppermost part of the Kuksha palaeoweathering crust. Unlike other metamorphosed-altered Archaean–(Palaeo) Proterozoic weathering crusts, the Kuksha palaeoweathering crust contains preserved kaolinitic clay, along with a muscovite-composition mica that possibly represents a recrystallized Al-rich smectitic phase precursor, and Fe-rich chlorite that has developed at the expense of Fe(II)-rich vermiculite and/or smectite.

The palaeo-pH AlCa proxy, although not directly applicable to Precambrian palaeoweathering crusts, exhibits pH values around 5.0–5.5 in the upper part of the Kuksha palaeoweathering crust. These indicate acidic weathering conditions under low-oxygen conditions suggested by the presence of rare-earth-element-rich phosphate rhabdophane and redox-sensitive element proxies.

The climofunctions suggest that the Kuksha palaeoweathering crust formed under cool temperate climate with mean annual temperatures ~12–13 °C and mean annual precipitation between 700 and 1100 mm yr^{-1}, roughly corresponding to modern Mediterranean climate. These palaeoclimate estimates agree with the palaeogeographic reconstructions of the Karelian craton between 30° and 40° latitudes at 2.4 Ga.

Despite the high weathering rates in temperate climate, the best palaeo-atmospheric pCO_2 values estimated for the Kuksha palaeoweathering crust range only within 1–10 PAL. The low pCO_2 levels could also be linked to the emergence of continental cratons above sea level, providing fresh basalts that sequestered CO_2 through silicate weathering, thus lessening the greenhouse effect and through that causing the initiation of the Huronian glaciation.

The Palaeoproterozoic sedimentary successions of the Seidorechka, Polisarka and Umba Sedimentary formations in the Imandra–Varzuga Greenstone Belt, northern Fennoscandian Shield, were deposited in continental rift setting.

Mixed mafic and Archaean granitized gneisses served as a provenance for the Seidorechka and Polisarka Sedimentary formations, whereas the Umba Sedimentary Formation is derived from more felsic provenance, possibly from the felsic volcanics of the Polisarka Volcanic Formation and Archaean gneisses.

The Polisarka Sedimentary Formation that deposited during the Huronian global glaciation is characterized by low chemical weathering intensity. Opposite to what was expected, there is no difference in overall silicate weathering intensity

indicators between the Seidorechka Sedimentary and Umba Sedimentary formations deposited, respectively, prior to and after the GOE and at the onset of oxidative weathering.

The results of this study suggest that the punctuated (sulphuric) acidic weathering, caused by oxidation of sulphide minerals that had accumulated on the Earth's surface under anoxic atmosphere, did not affect the long-term silicate weathering intensity. Instead, it seems that the overall silicate weathering decreased with dropping atmospheric pCO_2 levels during the Archaean–Proterozoic transition.

REFERENCES

Aitchison, J. (Ed.), 1986. The Statistical Analysis of Compositional Data. Springer Netherlands, Dordrecht.

Alfimova, N.A., Novoselov, A.A., Matrenichev, V., Filho, C.R.D.S., 2014. Conditions of subaerial weathering of basalts in the Neoarchean and Paleoproterozoic. Precambrian Res. 241, 1–16.

Amelin, Yu.V., Heaman, L.M., Semenov, V.S., 1995. U/Pb geochronology of layered mafic intrusions in the eastern Baltic Shield: implications for the timing and duration of Paleoproterozoic continental rifting. Precambrian Research 75, 31–46. https://doi.org/10.1016/0301-9268(95)00015-W

Arestova, N.A., Khramov, A.N., Gooskova, E.G., Iosifidi, A.G., 2002. New paleomagnetic evidence from the Early Proterozoic (2.5-2.4 Ga) Mount Generalskaya and Imandra layered intrusions, Kola Peninsula. Izvestiya, Physics of the Solid Earth 38, 233–243.

Arzamastsev, A.A., Egorova, S.V., Erofeeva, K.G., Samsonov, A.V., Stepanova, A.V., Skuf'in, P.K., Chashchin, V.V., Veselovskiy, R.V., 2020. Paleoproterozoic (2.51–2.40 Ga) Igneous Provinces of the Northeastern Fennoscandia: Geochemistry of Volcanic Rocks and Correlation with Intrusive Complexes. Stratigr. Geol. Correl. 28, 603–629. https://doi.org/10.1134/S0869593820060039

Babechuk, M.G., Widdowson, M., Kamber, B.S., 2014. Quantifying chemical weathering intensity and trace element release from two contrasting basalt profiles, Deccan Traps, India. Chemical Geology 363, 56–75. https://doi.org/10.1016/j.chemgeo.2013.10.027

Bachan, A., Kump, L.R., 2015. The rise of oxygen and siderite oxidation during the Lomagundi Event. Proceedings of the National Academy of Sciences 112, 6562–6567. https://doi.org/10.1073/pnas.1422319112

Bahlburg, H., Dobrzinski, N., 2011. A review of the Chemical Index of Alteration (CIA) and its application to the study of Neoproterozoic glacial deposits and climate transitions. Geological Society, London, Memoirs 36, 81–92.

Banfield, J.F., 1989. Apatite Replacement and Rare Earth Mobilization, Fractionation, and Fixation During Weathering. Clays and Clay Minerals 37, 113–127. https://doi.org/10.1346/CCMN.1989.0370202

Bazilevskaya, E., Rother, G., Mildner, D.F., Pavich, M., Cole, D., Bhatt, M.P., Jin, L., Steefel, C.I., Brantley, S.L., 2015. How oxidation and dissolution in diabase and granite control porosity during weathering. Soil Science Society of America Journal 79, 55–73.

Beaulieu, E., Goddëris, Y., Donnadieu, Y., Labat, D., Roelandt, C., 2012. High sensitivity of the continental-weathering carbon dioxide sink to future climate change. Nature Climate Change 2, 346–349. https://doi.org/10.1038/nclimate1419

Bekasova NB, Pushkin GY (1977) Allothigenic minerals of heavy fraction from metaterrigeneous rocks of the Imandra/Varzuga Zone. In: Sidorenko AV (ed) Lithology and geochemistry of the early precambrian. Kola Science Centre, Apatity, pp 33–44 (in Russian)

Bekker, A., Holland, H.D., Wang, P.-L., Rumble, D., Stein, H.J., Hannah, J.L., Coetzee, L.L., Beukes, N.J., 2004. Dating the rise of atmospheric oxygen. Nature 427, 117–120.

Brasier, A.T., Martin, A.P., Melezhik, V.A., Prave, A.R., Condon, D.J., Fallick, A.E., 2013. Earth's earliest global glaciation? Carbonate geochemistry and geochronology of the Polisarka Sedimentary Formation, Kola Peninsula, Russia. Precambrian Res. 235, 278–294.

Brimhall, G.H., Dietrich, W.E., 1987. Constitutive mass balance relations between chemical composition, volume, density, porosity, and strain in metasomatic hydrochemical systems: results on weathering and pedogenesis. Geochim. Cosmochim. Acta 51, 567–587.

Broecker, W., 2018. Co2: Earth's climate driver. Geochemical Perspectives 7, 117–194.

Buchan, K.L., 2014. Reprint of "Key paleomagnetic poles and their use in Proterozoic continent and supercontinent reconstructions: a review". Precambrian Res. 244 5–22.

Canfield, D.E., Ngombi-Pemba, L., Hammarlund, E.U., Bengtson, S., Chaussidon, M., Gauthier-Lafaye, F., Meunier, A., Riboulleau, A., Rollion-Bard, C., Rouxel, O., Asael, D., Pierson-Wickmann, A.-C., Albani, A.E., 2013. Oxygen dynamics in the aftermath of the Great Oxidation of Earth's atmosphere. PNAS 110, 16736–16741. https://doi.org/10.1073/pnas.1315570110

Cerling, T.E., 1984. The Stable Isotopic Composition of Modern Soil Carbonate and its Relationship to climate. Earth Planet. Sci. Lett. 71, 229–240.

Cerling, T.E., 1992. Use of carbon isotopes in paleosols as an indicator of the P(CO2) of the paleoatmosphere. Glob. Biogeochem. Cycles 6, 307–314.

Chashchin, V.V., Bayanova, T.B., Levkovich, N.V., 2008. Volcanoplutonic association of the early-stage evolution of the Imandra-Varzuga rift zone, Kola Peninsula, Russia: geological, petrogeochemical, and isotope-geochronological data. Petrology 16, 279–298.

Condie, K., 2001. Precambrian superplumes and supercontinents: a record in black shales, carbon isotopes, and paleoclimates? Precambrian Research 106, 239–260. https://doi.org/10.1016/S0301-9268(00)00097-8

Cotton, J.M., Sheldon, N.D., 2012. New constraints on using paleosols to reconstruct atmospheric pCO(2). Geol. Soc. Am. Bull. 124, 1411–1423.

Crockford, P.W., Kunzmann, M., Bekker, A., Hayles, J., Bao, H., Halverson, G.P., Peng, Y., Bui, T.H., Cox, G.M., Gibson, T.M., Wörndle, S., Rainbird, R., Lepland, A., Swanson-Hysell, N.L., Master, S., Sreenivas, B., Kuznetsov, A., Krupenik, V., Wing, B.A., 2019. Claypool continued: Extending the isotopic record of sedimentary sulfate. Chemical Geology 513, 200–225. https://doi.org/10.1016/j.chemgeo.2019.02.030

Dessert, C., Dupré, B., Gaillardet, J., François, L.M., Allègre, C.J., 2003. Basalt weathering laws and the impact of basalt weathering on the global carbon cycle. Chemical Geology 202, 257–273. https://doi.org/10.1016/j.chemgeo.2002.10.001

Driese, S.G., Ludvigson, G.A., Roberts, J.A., Fowle, D.A., González, L.A., Smith, J.J., Vulava, V.M., McKay, L.D., 2010. Micromorphology and stable-isotope geochemistry of historical pedogenic siderite formed in PAH-contaminated alluvial clay soils, Tennessee, USA. J. Sediment. Res. 80, 943–954.

Driese, S.G., Jirsa, M.A., Ren, M., Brantley, S.L., Sheldon, N.D., Parker, D., Schmitz, M., 2011. Neoarchean paleoweathering of tonalite and metabasalt: Implications for reconstructions of 2.69Ga early terrestrial ecosystems and paleoatmospheric chemistry. Precambrian Research 189, 1–17. https://doi.org/10.1016/j.precamres.2011.04.003

Driese, S.G., Medaris, L.G., Kirsimäe, K., Somelar, P., Stinchcomb, G.E., 2018. Oxisolic processes and geochemical constraints on duration of weathering for Neoproterozoic Baltic paleosol. Precambrian Res. 310, 165–178.

Ekart, D.D., Cerling, T.E., Montañez, I.P., Tabor, N.J., 1999. A 400 million year carbon isotope record of pedogenic carbonate: Implications for paleoatmospheric carbon dioxide. Am. J. Sci. 299, 805–827.

Fabre, S., Antonio, P.Y.J., Hir, G.L., 2021. Harsh or balmy weathering conditions onto the first continent surface? Precambrian Research 353, 106025. https://doi.org/10.1016/j.precamres.2020.106025

Fedo, C.M., Nesbitt, H.W., Young, G.M., 1995. Unraveling the effects of potassium metasomatism in sedimentary rocks and paleosols, with implications for paleo-weathering conditions and provenance. Geology 23, 921–924.

Feng, W., Yapp, C.J., 2009. Paleoenvironmental implications of concentration and 13C/12C ratios of Fe(CO3)OH in goethite from a mid-latitude Cenomanian laterite in southwestern Minnesota. Geochim. Cosmochim. Acta 73, 2559–2580.

Filippelli, G.M., 2011. Phosphate rock formation and marine phosphorus geochemistry: the deep time perspective. Chemosphere 84, 759–766.

Friedli, H., Lotscher, H., Oeschger, H., Siegenthaler, U., Stauffer, B., 1986. Ice Core Record of the C-13/C-12 Ratio of Atmospheric Co2 in the past 2 Centuries. Nature 324, 237–238.

Gäb, F., Ballhaus, C., Siemens, J., Heuser, A., Lissner, M., Geisler, T., Garbe-Schönberg, D., 2017. Siderite cannot be used as CO2 sensor for Archaean atmospheres. Geochim. Cosmochim. Acta 214, 209–225.

Gärtner, C., Bahlburg, H., Melezhik, V.A., Berndt, J., 2014. Dating Palaeoproterozoic glacial deposits of the Fennoscandian Shield using detrital zircons from the Kola Peninsula, Russia. Precambrian Research 246, 281–295. https://doi.org/10.1016/j.precamres.2014.03.014

Gaschnig, R.M., Rudnick, R.L., McDonough, W.F., Kaufman, A.J., Hu, Z., Gao, S., 2014. Onset of oxidative weathering of continents recorded in the geochemistry of ancient glacial diamictites. Earth and Planetary Science Letters 408, 87–99. https://doi.org/10.1016/j.epsl.2014.10.002

González-Álvarez, I., Kerrich, R., 2012. Weathering intensity in the Mesoproterozoic and modern large-river systems: A comparative study in the Belt-Purcell Supergroup, Canada and USA. Precambrian Research 208–211, 174–196. https://doi.org/10.1016/j.precamres.2012.04.008

Gumsley, A.P., Chamberlain, K.R., Bleeker, W., Söderlund, U., Kock, M.O. de, Larsson, E.R., Bekker, A., 2017. Timing and tempo of the Great Oxidation Event. PNAS 114, 1811–1816. https://doi.org/10.1073/pnas.1608824114

Hamer, J.M.M., Sheldon, N.D., Nichols, G.J., 2007. Global aridity during the early miocene? A terrestrial paleoclimate record from the Ebro basin, Spain. J. Geol. 115, 601–608.

Hanski, E.J., 2013. Evolution of the Palaeoproterozoic (2.50–1.95 Ga) Non-orogenic Magmatism in the Eastern Part of the Fennoscandian Shield. In: Melezhik, V.A., Prave, A.R., Hanski, E.J., Fallick, A.E., Lepland, A., Kump, L.R., Strauss, H. (Eds.), Reading the Archive of Earth's Oxygenation. Volume 1: The Palaeoproterozoic of Fennoscandia as Context for the Fennoscandian Arctic Russia - Drilling Early Earth Project. Springer, Berlin, Heidelberg, pp. 179-245.

Hao, J., Knoll, A.H., Huang, F., Hazen, R.M., Daniel, I., 2020. Cycling Phosphorus on the Archean Earth: Part I. Continental weathering and riverine transport of phosphorus. Geochimica et Cosmochimica Acta. https://doi.org/10.1016/j.gca.2020.01.027

Hao, J., Sverjensky, D.A., Hazen, R.M., 2017. Mobility of nutrients and trace metals during weathering in the late Archean. Earth and Planetary Science Letters 471, 148–159. https://doi.org/10.1016/j.epsl.2017.05.003

Hao, W., Mänd, K., Li, Y., Alessi, D.S., Somelar, P., Moussavou, M., Romashkin, A.E., Lepland, A., Kirsimäe, K., Planavsky, N.J., Konhauser, K.O., 2021. The kaolinite shuttle links the Great Oxidation and Lomagundi events. Nature Communications 12, 2944. https://doi.org/10.1038/s41467-021-23304-8

Hayashi, K.-I., Fujisawa, H., Holland, H.D., Ohmoto, H., 1997. Geochemistry of ~1.9 Ga sedimentary rocks from northeastern Labrador. Canada. *Geochimica et Cosmochimica Acta* 61 (19), 4115–4137. https://doi.org/10.1016/S0016-7037(97)00214-7.

Hayes, N.R., Buss, H.L., Moore, O.W., Krám, P., Pancost, R.D., 2020. Controls on granitic weathering fronts in contrasting climates. Chemical Geology 535, 119450. https://doi.org/10.1016/j.chemgeo.2019.119450

Hazen, R.M., Papineau, D., Bleeker, W., Downs, R.T., Ferry, J.M., McCoy, T.J., Sverjensky, D.A., Yang, H., 2008. Mineral evolution. American Mineralogist 93, 1693–1720. https://doi.org/10.2138/am.2008.2955

Herron, M.M., 1988. Geochemical classification of terrigenous sands and shales from core or log data.

Hoffman, P.F., Abbot, D.S., Ashkenazy, Y., Benn, D.I., Brocks, J.J., Cohen, P.A., Cox, G.M., Creveling, J.R., Donnadieu, Y., Erwin, D.H., Fairchild, I.J., Ferreira, D., Goodman, J.C., Halverson, G.P., Jansen, M.F., Le Hir, G., Love, G.D., Macdonald, F.A., Maloof, A.C., Partin, C.A., Ramstein, G., Rose, B.E.J., Rose, C.V., Sadler, P.M., Tziperman, E., Voigt, A., Warren, S.G., 2017. Snowball Earth climate dynamics and Cryogenian geology-geobiology. Sci. Adv. 3.

Holland, H.D., 2006. The oxygenation of the atmosphere and oceans. Philosophical Transactions of the Royal Society B: Biological Sciences 361, 903–915. https://doi.org/10.1098/rstb.2006.1838

Homann, M., Sansjofre, P., Van Zuilen, M., Heubeck, C., Gong, J., Killingsworth, B., Foster, I.S., Airo, A., Van Kranendonk, M.J., Ader, M., Lalonde, S.V., 2018. Microbial life and biogeochemical cycling on land 3,220 million years ago. Nat. Geosci. 11, 665.

Kanzaki, Y., Murakami, T., 2015. Estimates of atmospheric CO2 in the Neoarchean–Paleoproterozoic from paleosols. Geochimica et Cosmochimica Acta 159, 190–219. https://doi.org/10.1016/j.gca.2015.03.011

Kanzaki, Y., Murakami, T., 2018a. Effects of atmospheric composition on apparent activation energy of silicate weathering: I. Model formulation. Geochim. Cosmochim. Acta 233, 159–186.

Kanzaki, Y., Murakami, T., 2018b. Effects of atmospheric composition on apparent activation energy of silicate weathering: II. Implications for evolution of atmospheric CO2 in the Precambrian. Geochim. Cosmochim. Acta 240, 314–330.

Karhu, J.A., Holland, H.D., 1996. Carbon isotopes and the rise of atmospheric oxygen. Geology 24, 867–870.

Kasting, J.F., 1987. Theoretical constraints on oxygen and carbon dioxide concentrations in the Precambrian atmosphere. Precambrian Research 34, 205–229. https://doi.org/10.1016/0301-9268(87)90001-5

Kholodov, V.N., Butuzova, G.Y., 2008. Siderite formation and evolution of sedimentary iron ore deposition in the Earth's history. Geol. Ore Deposits 50, 299. https://doi.org/10.1134/S107570150804003X

Kim, H., Stinchcomb, G., Brantley, S.L., 2017. Feedbacks among O2 and CO2 in deep soil gas, oxidation of ferrous minerals, and fractures: A hypothesis for steady-state regolith thickness. Earth and Planetary Science Letters 460, 29–40. https://doi.org/10.1016/j.epsl.2016.12.003

Kirsimäe, K., Melezhik, V.A., 2013. Palaeoproterozoic weathered surfaces. In: Melezhik, V.A., Kump, L.R., Fallick, A.E., Strauss, H., Hanski, E.J., Prave, A.R., Lepland, A. (Eds.), Reading the Archive of Earth's Oxygenation. Volume 3: Global Events and the Fennoscandian Arctic Russia – Drilling Early Earth Project. Springer, Berlin, Heidelberg, pp. 1409–1418.

Kirschvink, J.L., Gaidos, E.J., Bertani, L.E., Beukes, N.J., Gutzmer, J., Maepa, L.N., Steinberger, R.E., 2000. Paleoproterozoic snowball Earth: Extreme climatic and geochemical global change and its biological consequences. Proc. Natl. Acad. Sci. U.S.A. 97, 1400–1405.

Kopp, R.E., Kirschvink, J.L., Hilburn, I.A., Nash, C.Z., 2005. The Paleoproterozoic snowball Earth: a climate disaster triggered by the evolution of oxygenic photosynthesis. Proc. Natl. Acad. Sci. U. S. A. 102, 11131–11136.

Konhauser, K.O., Lalonde, S.V., Planavsky, N.J., Pecoits, E., Lyons, T.W., Mojzsis, S.J., Rouxel, O.J., Barley, M.E., Rosìere, C., Fralick, P.W., Kump, L.R., Bekker, A., 2011. Aerobic bacterial pyrite oxidation and acid rock drainage during the Great Oxidation Event. Nature 478, 369–373. https://doi.org/10.1038/nature10511

Kump, L.R., Brantley, S.L., Arthur, M.A., 2000. Chemical Weathering, Atmospheric CO2, and Climate. Annu. Rev. Earth Planet. Sci. 28, 611–667. https://doi.org/10.1146/annurev.earth.28.1.611

Laakso, T.A., Schrag, D.P., 2018. Limitations on Limitation. Global Biogeochemical Cycles 32, 486–496. https://doi.org/10.1002/2017GB005832

Laajoki, K., 2005. Karelian supracrustal rocks. In: Lehtinen, M., Nurmi, P.A., Rämö, O.T. (Eds.), Precambrian Geology of Finland – Key to the Evolution of the Fennoscandian Shield. Elsevier B.V., Amsterdam, pp. 279–342.

Laajoki, K., Strand, K., Härmä, P., 1989. Lithostratigraphy of the early Proterozoic Kainuu Schist belt in the Kurkikylä Siikavaara area, northern Finland, with emphasis on the genetic approach. Geol. Soc. Finland Bull. 61, 65–93.

Li, C., Yang, S., 2010. Is chemical index of alteration (CIA) a reliable proxy for chemical weathering in global drainage basins? American Journal of Science 310, 111–127. https://doi.org/10.2475/02.2010.03

Li, S., Gaschnig, R.M., Rudnick, R.L., 2016. Insights into chemical weathering of the upper continental crust from the geochemistry of ancient glacial diamictites. Geochimica et Cosmochimica Acta 176, 96–117. https://doi.org/10.1016/j.gca.2015.12.012

Liivamägi, S., Somelar, P., Vircava, I., Mahaney, W.C., Kirs, J., Kirsimäe, K., 2015. Petrology, mineralogy and geochemical climofunctions of the Neoproterozoic Baltic paleosol. Precambrian Res. 256, 170–188.

Lipp, A.G., Shorttle, O., Sperling, E.A., Brocks, J.J., Cole, D.B., Crockford, P.W., Del Mouro, L., Dewing, K., Dornbos, S.Q., Emmings, J.F., Farrell, U.C., Jarrett, A., Johnson, B.W., Kabanov, P., Keller, C.B., Kunzmann, M., Miller, A.J., Mills, N.T., O'Connell, B., Peters, S.E., Planavsky, N.J., Ritzer, S.R., Schoepfer, S.D., Wilby, P.R., Yang, J., 2021. The composition and weathering of the continents over geologic time. Geochemical Perspectives Letters 21–26. https://doi.org/10.7185/ geochemlet.2109.

Lipp, A. G., Shorttle, O., Syvret, F., & Roberts, G. G. (2020). Major Element Composition of Sediments in Terms of Weathering and Provenance: Implications for Crustal Recycling. *Geochemistry, Geophysics, Geosystems*, *21*(6), e2019GC008758. https:// doi.org/10.1029/2019GC008758.

Lowe, D.R., Tice, M.M., 2004. Geologic evidence for Archean atmospheric and climatic evolution: Fluctuating levels of CO2, CH4, and O-2, with an overriding tectonic control. Geology 32, 493–496.

Lowe, D.R., Tice, M.M., 2007. Tectonic controls on atmospheric, climatic, and biological evolution 3.5–2.4 Ga. Precambrian Research, Earliest Evidence of Life on Earth 158, 177–197. https://doi.org/10.1016/j.precamres.2007.04.008

Lubnina, N.V., Slabunov, A.I., 2017. The Karelian Craton in the Structure of the Kenorland Supercontinent in the Neoarchean: New Paleomagnetic and Isotope Geochronology Data on Granulites of the Onega Complex. Moscow Univ. Geol. Bull. 72, 377–390. https://doi.org/10.3103/S0145875217060072

Ludvigson, G.A., Gonzalez, L.A., Metzger, R.A., Witzke, B.J., Brenner, R.L., Murillo, A.P., White, T.S., 1998. Meteoric sphaerosiderite lines and their use for paleohydrology and paleoclimatology. Geology 26, 1039–1042.

Lukens, W.E., Nordt, L.C., Stinchcomb, G.E., Driese, S.G., Tubbs, J.D., 2018. Reconstructing pH of Paleosols Using Geochemical Proxies. The Journal of Geology 126, 427–449. https://doi.org/10.1086/697693

Luo, G., Ono, S., Beukes, N.J., Wang, D.T., Xie, S., Summons, R.E., 2016. Rapid oxygenation of Earth's atmosphere 2.33 billion years ago. Sci Adv 2. https://doi.org/10.1126/sciadv.1600134

Lyons, T.W., Reinhard, C.T., Planavsky, N.J., 2014. The rise of oxygen in Earth's early ocean and atmosphere. Nature 506, 307–315. https://doi.org/10.1038/nature13068

Mänd, K., Lalonde, S.V., Robbins, L.J., Thoby, M., Paiste, K., Kreitsmann, T., Paiste, P., Reinhard, C.T., Romashkin, A.E., Planavsky, N.J., Kirsimäe, K., Lepland, A., Konhauser, K.O., 2020. Palaeoproterozoic oxygenated oceans following the Lomagundi–Jatuli Event. Nat. Geosci. 13, 302–306. https://doi.org/10.1038/s41561-020-0558-5

Mack, G.H., James, W.C., 1994. Paleoclimate and the Global distribution of Paleosols. The Journal of Geology 102, 360–366.

Marshall, H.G., Walker, J.C.G., Kuhn, W.R., 1988. Long-term climate change and the geochemical cycle of carbon. Journal of Geophysical Research: Atmospheres 93, 791–801. https://doi.org/10.1029/JD093iD01p00791

Martin, A.P., Condon, D.J., Prave, A.R., Melezhik, V.A., Lepland, A., Fallick, A.E., 2013a. Dating the termination of the Palaeoproterozoic Lomagundi-Jatuli carbon isotopic event in the North Transfennoscandian Greenstone Belt. Precambrian Res. 224, 160–168.

Martin, A.P., Condon, D.J., Prave, A.R., Lepland, A., 2013b. A review of temporal constraints for the Palaeoproterozoic large, positive carbonate carbon isotope excursion (the Lomagundi-Jatuli Event). Earth Sci. Rev. 127, 242–261. https://doi.org/10.1016/j.earscirev.2013.10.006.

Martin, A.P., Prave, A.R., Condon, D.J., Lepland, A., Fallick, A.E., Romashkin, A.E., Medvedev, P.V., Rychanchik, D.V., 2015. Multiple Palaeoproterozoic carbon burial episodes and excursions. Earth Planet. Sci. Lett. 424, 226–236.

Mattos, N.H.S., Batezelli, A., 2019. Source-area, paleoweathering and provenance of the late Cretaceous sequences of the Bauru Basin (SE Brazil). Geociencias 38, 943–960. https://doi.org/10.5016/geociencias.v38i4.10565

Maynard, J.B., 1992. Chemistry of modernsoils as a guide to interpreting Precambrian paleosols. J. Geol. 100, 279–289.

McLennan, S. M., Hemming, S., McDaniel, D. K., & Hanson, G. N. (1993). Geochemical approaches to sedimentation, provenance, and tectonics. Geological Society of America Special Papers. 284, 21–40. https://doi.org/10.1130/SPE284-p21

Medaris, L.G., Driese, S.G., Stinchcomb, G.E., 2017. The Paleoproterozoic Baraboo paleosol revisited: Quantifying mass fluxes of weathering and metasomatism, chemical climofunctions, and atmospheric p CO 2 in a chemically heterogeneous protolith. Precambrian Research 301, 179–194. https://doi.org/10.1016/j.precamres.2017.06.010

Medaris, L.G., Driese, S.G., Stinchcomb, G.E., Fournelle, J.H., Lee, S., Xu, H., DiPietro, L.M., Gopon, P., Stewart, E.K., 2018. Anatomy of a sub–Cambrian paleosol in Wisconsin: mass fluxes of chemical weathering and climatic conditions in North America during formation of the Great Cambrian Unconformity. J. Geol. 126, 261–283.

Melezhik, V.A. (Ed.), 2013. The Core Archive of the Fennoscandian Arctic Russia – Drilling Early Earth Project, Reading the archive of earth's oxygenation. Springer, Berlin.

Melezhik, V.A., Hanski, E.J., 2013. The Early Palaeoproterozoic of Fennoscandia: Geological and Tectonic Settings. In: Melezhik, V.A., Prave, A.R., Hanski, E.J., Fallick, A.E., Lepland, A., Kump, L.R., Strauss, H. (Eds.), Reading the Archive of Earth's Oxygenation. Volume 1: The Palaeoproterozoic of Fennoscandia as Context for the Fennoscandian Arctic Russia - Drilling Early Earth Project. Springer, Berlin, Heidelberg, pp. 33-39.

Melezhik, V.A., Fallick, A.E., 1996. A widespread positive ? $^{13}C_{carb}$ anomaly at around 2.33?2.06 Ga on the Fennoscandian Shield: a paradox? Terra Nova 8, 141–157. https://doi.org/10.1111/j.1365-3121.1996.tb00738.x

Melezhik, V.A., Fallick, A.E., Filippov, M.M., Larsen, O., 1999. Karelian shungite—an indication of 2.0-Ga-old metamorphosed oil-shale and generation of petroleum: geology, lithology and geochemistry. Earth-Science Reviews 47, 1–40.

Melezhik, V.A., Sturt, B.A., 1994. General geology and evolutionary history of the early proterozoic Polmak-Pasvik-Pechenga-Imandra/Varzuga-Ust'Ponoy greenstone belt in the northeastern Baltic Shield. Earth-Science Reviews 36, 205–241. https://doi.org/10.1016/0012-8252(94)90058-2

Melezhik VA, Borisov AE, Fedotov ZhA, Predovsky AA (1982) The Varzuga series. In: Gorbunov GI (ed) The Imandra/Varzuga Zone of the Karelides. Nauka (Science), Leningrad, pp 57–85 (in Russian)

Mertanen, S., Pesonen, L.J., 2005. Chapter 15 Drift history of the shield, in: Lehtinen, M., Nurmi, P.A., Rämö, O.T. (Eds.), Developments in Precambrian Geology, Precambrian Geology of Finland Key to the Evolution of the Fennoscandian Shield. Elsevier, pp. 645–668. https://doi.org/10.1016/S0166-2635(05)80016-7

Mertanen, S., Vuollo, J.I., Huhma, H., Arestova, N.A., Kovalenko, A., 2006. Early Paleoproterozoic–Archean dykes and gneisses in Russian Karelia of the Fennoscandian Shield—New paleomagnetic, isotope age and geochemical investigations. Precambrian Research 144, 239–260. https://doi.org/10.1016/j.precamres.2005.11.005

Mertanen, S., Korhonen, F., 2011. Paleomagnetic constraints on an Archean –Paleoproterozoic Superior–Karelia connection: new evidence from Archean Karelia Precambrian Res. 186, 193–204.

Meunier, A., Sardini, P., Robinet, J.C., Prêt, D., 2007. The petrography of weathering processes: facts and outlooks. Clay Minerals 42, 415–435. https://doi.org/10.1180/claymin.2007.042.4.01

Mills, B., Lenton, T.M., Watson, A.J., 2014. Proterozoic oxygen rise linked to shifting balance between seafloor and terrestrial weathering. PNAS 111, 9073–9078. https://doi.org/10.1073/pnas.1321679111

Mills, B.J.W., Krause, A.J., Scotese, C.R., Hill, D.J., Shields, G.A., Lenton, T.M., 2019. Modelling the long-term carbon cycle, atmospheric CO2, and Earth surface temperature from late Neoproterozoic to present day. Gondwana Research 67, 172–186. https://doi.org/10.1016/j.gr.2018.12.001

Mitchell, R.L., Sheldon, N.D., 2010. The ~1100Ma Sturgeon Falls paleosol revisited: Implications for Mesoproterozoic weathering environments and atmospheric CO2 levels. Precambrian Research 183, 738–748. https://doi.org/10.1016/j.precamres.2010.09.003

Mohanty, S.P., Nanda, S., 2016. Geochemistry of a paleosol horizon at the base of the Sausar Group, central India: Implications on atmospheric conditions at the Archean–Paleoproterozoic boundary. Geoscience Frontiers 7, 759–773. https://doi.org/10.1016/j.gsf.2015.10.002

Murakami, T., Ito, J.-I., Utsunomiya, S., Kasama, T., Kozai, N., Ohnuki, T., 2004. Anoxic dissolution processes of biotite: implications for Fe behavior during Archean weathering. Earth and Planetary Science Letters 224, 117–129. https://doi.org/10.1016/j.epsl.2004.04.040

Murakami, T., Utsunomiya, S., Imazu, Y., Prasad, N., 2001. Direct evidence of late Archean to early Proterozoic anoxic atmosphere from a product of 2.5 Ga old weathering. Earth and Planetary Science Letters 184, 523–528. https://doi.org/10.1016/S0012-821X(00)00344-7

Murakami, T., Matsuura, K., Kanzaki, Y., 2016. Behaviors of trace elements in Neoarchean and Paleoproterozoic paleosols: Implications for atmospheric oxygen evolution and continental oxidative weathering. Geochimica et Cosmochimica Acta 192, 203–219. https://doi.org/10.1016/j.gca.2016.07.008.

Nedachi, Y., Nedachi, M., Bennett, G., Ohmoto, H., 2005. Geochemistry and mineralogy of the 2.45 Ga Pronto paleosols, Ontario, Canada. Chemical Geology 214, 21–44. https://doi.org/10.1016/j.chemgeo.2004.08.026

Nesbitt, H.W., Markovics, G., price, R.C., 1980. Chemical processes affecting alkalis and alkaline earths during continental weathering. Geochimica et Cosmochimica Acta 44, 1659–1666. https://doi.org/10.1016/0016-7037(80)90218-5

Nesbitt, H.W., Young, G.M., 1982. Early proterozoic climates and plate motion inferred from major element chemistry of lutites. Nature 299.

Nesbitt, H.W., Young, G.M., 1984. Prediction of some weathering trends of plutonic and volcanic rocks based on thermodynamic and kinetic conciderations. Geochimica et Cosmochimica Acta 48, 1523-1534.

Nykänen, V.M., Vuollo, J.I., Liipo, J.P., Piirainen, T.A., 1994. Transitional (2.1 Ga) Fetholeiitic-tholeiitic magmatism in the Fennoscandian Shield signifying lithospheric thinning during Paleoproterozoic extensional tectonics. Reecambriang Research 70, 45-65.

Ohmoto, H., Watanabe, Y., Kumazawa, K., 2004. Evidence from massive siderite beds for a CO2-rich atmosphere before ,1.8 billion years ago. Nature 429, 395–399. https://doi.org/10.1038/nature02572

Ohmoto, H., Watanabe, Y., Lasaga, A.C., Naraoka, H., Johnson, I., Brainard, J., Chorney, A., 2014. Oxygen, iron, and sulfur geochemical cycles on early Earth: Paradigms and contradictions. Earth's Early Atmosphere and Surface Environment 504, 55–95.

Ojakangas, R.W., Marmo, J.S., Heiskanen, K.I., 2001. Basin evolution of the Paleoproterozoic Karelian Supergroup of the Fennoscandian (Baltic) shield. Sedimentary Geology 141, 255–285.

Oze, C., Bird, D.K., Fendorf, S., 2007. Genesis of hexavalent chromium from natural sources in soil and groundwater. PNAS 104, 6544–6549. https://doi.org/10.1073/pnas.0701085104

Parker, A., 1970. An index of weathering for silicate rocks. Geological Magazine 107, 501–504.

Partin, C.A., Bekker, A., Planavsky, N.J., Scott, C.T., Gill, B.C., Li, C., Podkovyrov, V., Maslov, A., Konhauser, K.O., Lalonde, S.V., Love, G.D., Poulton, S.W., Lyons, T.W., 2013. Large-scale fluctuations in Precambrian atmospheric and oceanic oxygen levels from the record of U in shales. Earth and Planetary Science Letters 369–370, 284–293. https://doi.org/10.1016/j.epsl.2013.03.031

Poulton, S.W., Bekker, A., Cumming, V.M., Zerkle, A.L., Canfield, D.E., Johnston, D.T., 2021. A 200-million-year delay in permanent atmospheric oxygenation. Nature 592, 232–236. https://doi.org/10.1038/s41586-021-03393-7

Reinhard, C.T., Olson, S.L., Turner, S.K., Palike, C., Kanzaki, Y., Ridgwell, A., 2020. Oceanic and atmospheric methane cycling in the cGENIE Earth system model. arXiv:2007.15053 [astro-ph, physics:physics].

Retallack, G.J., 2001. Soils of the Past: An Introduction to Paleopedology. Blackwell Science, Oxford

Retallack, G.J., Noffke, N., 2019. Are there ancient soils in the 3.7 Ga Isua GreenstoneBelt, Greenland? Palaeogeogr. Palaeoclimatol. Palaeoecol. 514, 18–30.

Roser, B.P., Korsch, R.J., 1988. Provenance signatures of sandstone-mudstone suites determined using discriminant function analysis of major-element data. Chem. Geol. 67 (1), 119–139. https://doi.org/10.1016/0009-2541(88)90010-1.

Royer, D.L., 1999. Depth to pedogenic carbonate horizon as a paleoprecipitation indicator? Geology 27, 1123–1126.

Royer, D.L., 2014. 6.11 – Atmospheric CO2 and O2 during the Phanerozoic: Tools, patterns, and Impacts. In: Holland, H.D., Turekian, K.K. (Eds.), Treatise on Geochemistry, Second edition. Elsevier, Oxford, pp. 251–267.

Royer, D.L., Berner, R.A., Beerling, D.J., 2001. Phanerozoic atmospheric CO2 change: evaluating geochemical and paleobiological approaches. Earth Sci. Rev. 54, 349–392.

Rudnick, R.L., Gao, S., 2014.Composition of the Continental crust. Treatise on Geochemistry (Second Edition). 4, 1–51. https://doi.org/10.1016/B978-0-08-095975-7.00301-6

Rye, R., Holland, H.D., 2000. Geology and geochemistry of paleosols developed on the Hekpoort Basalt, Pretoria Group, South Africa. American Journal of Science 300, 85–141.

Sawicki, J., 1995. Microbial precipitation od siderite and protoferrihydrite in a biofilm. The Canadian Mineralogist 33, 6.

Scott, C., Lyons, T.W., Bekker, A., Shen, Y., Poulton, S.W., Chu, X., Anbar, A.D., 2008. Tracing the stepwise oxygenation of the Proterozoic ocean. Nature 452, 456–459. https://doi.org/10.1038/nature06811

Sheldon, N.D., Retallack, G.J., Tanaka, S., 2002. Geochemical climofunctions from north American soils and application to paleosols across the Eocene-Oligocene boundary in Oregon. J. Geol. 110, 687–696.

Sheldon, N.D., 2006. Precambrian paleosols and atmospheric CO2 levels. Precambrian Research 147, 148–155. https://doi.org/10.1016/j.precamres.2006.02.004

Sheldon, N.D., Tabor, N.J., 2009. Quantitative paleoenvironmental and paleoclimatic reconstruction using paleosols. Earth-Science Reviews 95, 1–52. https://doi.org/10.1016/j.earscirev.2009.03.004

Skyttä, P., Piippo, S., Kloppenburg, A., Corti, G., 2019. 2. 45 Ga break-up of the Archaean continent in Northern Fennoscandia: Rifting dynamics and the role of inherited structures within the Archaean basement. Precambrian Research 324, 303–323. https://doi.org/10.1016/j.precamres.2019.02.004

Smit, M.A., Mezger, K., 2017. Earth's early O2 cycle suppressed by primitive continents. Nature Geoscience 10, 788–792. https://doi.org/10.1038/ngeo3030

Smolkin, V.F., Mezhelovskaya, S.V., Mezhelovsky, A.D., 2020. The Sources of the Clastic Material of the Terrigenous Sequences of the Neoarchean and Paleoproterozoic Paleobasins in the Eastern Part of the Fennoscandian Shield Based on Isotope Analysis Data for Detrital Zircons (SIMS, LA-ICP-MS). Stratigr. Geol. Correl. 28, 571–602. https://doi.org/10.1134/S086959382006009X

Somelar, P., Soomer, S., Driese, S.G., Lepland, A., Stinchcomb, G.E., Kirsimäe, K., 2020. CO2 drawdown and cooling at the onset of the Great Oxidation Event recorded in 2.45 Ga paleoweathering crust. Chemical Geology 548, 119678. https://doi.org/10.1016/j.chemgeo.2020.119678.

Soomer, S., Somelar, P., Mänd, K., Driese, S.G., Lepland, A., Kirsimäe, K., 2019. High-CO2, acidic and oxygen-starved weathering at the Fennoscandian Shield at the Archean-Proterozoic transition. Precambr. Res. 327, 68–80. https://doi.org/ 10.1016/j.precamres.2019.03.001.

Srivastava, P., Bhattacharyya, T., Pal, D.K., 2002. Significance of the formation of calcium carbonate minerals in the pedogenesis and management of cracking clay soils (vertisols) of India. Clay Clay Miner. 50, 111–126.

Stinchcomb, G.E., Nordt, L.C., Driese, S.G., Lukens, W.E., Williamson, F.C., Tubbs, J.D., 2016. A data-driven spline model designed to predict paleoclimate using paleosol geochemistry. Am. J. Sci. 316, 746–777.

Stinchcomb, G.E., Kim, H., Hasenmueller, E.A., Sullivan, P.L., Sak, P.B., Brantley, S.L., 2018. Relating soil gas to weathering using rock and regolith geochemistry. American Journal of Science 318, 727–763.

Sturt, B.A., Melezhik, V.A., Ramsay, D.M., 1994. Early Proterozoic regolith at Pasvik, NE Norway: palaeoenvironmental implications for the Baltic Shield. Terra Nova 6, 618–633. https://doi.org/10.1111/j.1365-3121.1994.tb00528.x

Tabor, N.J., Yapp, C.J., Montañes, I.P., 2004. Goethite, calcite, and organic matter from Permian and Triassic soils: carbon isotopes and CO2 concentrations. Geochim. Cosmochim. Acta 68, 1503–1517.

Taylor, J.C., 1991. Computer programs for standardless quantitative analysis of minerals using the full powder diffraction profile. Powder Diffr. 6, 2–9.

Taylor, S.R., McLennan, S.M., 1985. The continental crust: Its composition and evolution. N. p, United States.

Teitler, Y., Philippot, P., Gérard, M., Le Hir, G., Fluteau, F., Ader, M., 2015. Ubiquitous occurrence of basaltic-derived paleosols in the Late Archean Fortescue Group, Western Australia. Ubiquitous occurrence of basaltic-derived paleosols in the Late Archean Fortescue Group, Western Australia 267, 1–27.

Torrent, J., 2005. Mediterranean soils. In: Hillel, D. (Ed.), Encyclopedia of Soils in theEnvironment. Elsevier, Oxford, pp. 418–427.

Tosca, N.J., Johnston, D.T., Mushegian, A., Rothman, D.H., Summons, R.E., Knoll, A.H., 2010. Clay mineralogy, organic carbon burial, and redox evolution in Proterozoic oceans. Geochimica et Cosmochimica Acta 74, 1579–1592. https://doi.org/10.1016/j.gca.2009.12.001

Verma, S.P., Armstrong-Altrin, J.S., 2013. New multi-dimensional diagrams for tectonic discrimination of siliciclastic se Verma, S.P., Armstrong-Altrin, J.S., 2013. New multi-dimensional diagrams for tectonic discrimination of siliciclastic sediments and their application to Precambrian basins. Chem. Geol. 355, 117–133. https://doi.org/10.1016/j.chemgeo.2013.07.014.
diments and their application to Precambrian basins. Chem. Geol. 355, 117–133. https://doi.org/10.1016/j.chemgeo.2013.07.014.

Walker, J.C.G., Hays, P.B., Kasting, J.F., 1981. A negative feedback mechanism for the long-term stabilization of Earth's surface temperature. J. Geophys. Res. 86, 9776–9782.

Warke, M.R., Rocco, T.D., Zerkle, A.L., Lepland, A., Prave, A.R., Martin, A.P., Ueno, Y., Condon, D.J., Claire, M.W., 2020. The Great Oxidation Event preceded a Paleoproterozoic "snowball Earth." PNAS 117, 13314–13320. https://doi.org/10.1073/pnas.2003090117

Watanabe, Y., Martini, J.E.J., Ohmoto, H., 2000. Geochemical evidence for terrestrial ecosystems 2.6 billion years ago. Nature 408, 574–578.
Wilson, M.J., 2004. Weathering of the primary rock-forming minerals: processes, products and rates. Clay Minerals 39, 233–266. https://doi.org/10.1180/0009855043930133
Winnick, M.J., Maher, K., 2018. Relationships between CO2, thermodynamic limits on silicate weathering, and the strength of the silicate weathering feedback. Earth and Planetary Science Letters 485, 111–120. https://doi.org/10.1016/j.epsl.2018.01.005
Young, G.M., 2019. Aspects of the Archean-Proterozoic transition: How the great Huronian Glacial Event was initiated by rift-related uplift and terminated at the rift-drift transition during break-up of Lauroscandia. Earth-Science Reviews 190, 171–189. https://doi.org/10.1016/j.earscirev.2018.12.013
Young, G.M., 2013. Secular changes at the Earth's surface; evidence from palaeosols, some sedimentary rocks, and palaeoclimatic perturbations of the Proterozoic Eon. Gondwana Research 24, 453–467. https://doi.org/10.1016/j.gr.2012.07.016

SUMMARY IN ESTONIAN

Paleomurenemine Arhaikumi-Proterosoikumi üleminekul Imandra-Varzuga rohekilda vööndis Loode-Venemaal

Maa ajaloos märgilise tähtsusega perioodi – Arhaikumi – Proterosoikumi üleminekut, ligikaudu 2,4 miljardit aastat tagasi – markeerib vaba hapniku ilmumine Maa atmosfääri. Seda sündmust nimetatakse Suureks Hapnikusündmuseks (*Great Oxygenation Event – GOE*, Holland, 2002). Hapnikulise atmosfääri tekkimine tõi kaasa põhimõttelised muutused Maa geokeemilistes aineringetes ning sealhulgas käivitas laiaulatusliku kontinentaalsete kivimite oksüdatiivse murenemise. Seniste seisukohtade põhjal on arvatud, et anoksilistes tingimustes maapinnale kuhjunud sulfiidsete mineraalide lahustumine ja oksüdeerumine põhjustas hapnikuliste tingimuste tekkides intensiivse (väävel-)happelise murenemisimpulsi, mis omakorda kutsus esile erinevate toitainete plahvatusliku sissekande ookeanidesse, soodustades seeläbi veelgi primaarproduktsiooni ning fotosünteetilise hapniku tootmist. Murenemisprotsessi intensiivsus sõltub klimaatilistest tingimustest (nt sademed, temperatuur jm.) ning eriti süsinikdioksiidi (CO_2) osakaalust atmosfääris, mis mõjutab sademete happelisust ja kasvuhoone efekti kaudu kaudselt kogu Maa kliimat. Seevastu aga geoloogilises ajaskaalas intensiivsem kontinentaalne silikaatsete kivimite keemiline murenemine hoopis tasakaalustab kasvuhoone efekti, sidudes CO_2 merelistesse karbonaatidesse ning vähendades seeläbi CO_2 osakaalu atmosfääris.

Maa GOE järgsetes setendites/kivimites ja murenemiskoorikutes annavad atmosfäärse hapniku ilmumisest ja kontsentratsioonide järkjärgulisest kasvust märku paljude redutseeritud reaktiivsete mineraalide, nagu püriidi (FeS_2), uraniniidi (UO_2) ja sideriidi ($FeCO_3$) kadumine ning kolmevalentset rauda sisaldavate mineraalide, nagu hematiit (Fe_2O_3) ja götiit [$Fe^{3+}O(OH)$] ilmumine. Samas üheks olulisemaks vaba hapniku ilmumisele viitavaks tunnuseks on väävli isotoopide massist sõltumatu fraktsioneerumise signaali (*Mass-Independent Fractionation* - MIF) kadumine settekivimites, mis tekkisid 2,3 – 2,4 miljardit aastat tagasi. MIF signaali kadumine markeerib madalat, kuid kindlat hapniku sisaldust atmosfääris, mis on 0,001% tänapäevasest atmosfääri hapniku hulgast. Hapniku ilmumisega seotud võimalikule happerünnakule viitavad kivimis: ainult happelistes tingimustes (pH <5) lahustatava Cr rikastumine Paleoproterosoikumi meresetetes, redokstundlike elementide Mo ja U leostumine paleomuldadest merelistesse savikivimitesse ja fosfori leostumine paleomuldadest ning paleomuldade/meresetete oletatav kaoliniidi rikkus. Ometigi ei ole tänaseni selge kui laiaulatuslik oli võimaliku GOE happerünnaku mõju, sest erinevused murenemiskoorikute ja setete murenemisindeksites (nagu näiteks *CIA – Chemical Index of Alteration*) enne ja pärast GOE-d on väga väikesed või puuduvad hoopis. Selgete erinevuste puudumist murenemisintensiivsustes on põhjendatud nii selle ajaperioodi sette-

läbilõigete ebapiisava uuritusega, erinevustega lähtekivimi päritolus, tektooniliste ja paleogeograafiliste tegurite varieeruvusega kui ka settimisjärgsete digeneetiliste ja moondeprosessidega.

Kuna paleomullad tekivad otseses kontaktis atmosfääriga, peegeldavad nad tekkeaegseid keskkonnatingimusi, atmosfääri koostist ja on ainsad otsesed allikad kontinentaalsete murenemisprotsesside hindamiseks. Paleomuldade kaudu on võimalik hinnata murenemise intensiivsust, setendite kujunemise tektoonilist situatsiooni, lähtekivimi koostist. Klimaatilisi tingimusi on võimalik määrata ka terrigeensete settekivimite abil, mis sisaldavad murenemise käigus moodustunud, erodeeritud, transporditud ja ladestatud setteosakesi.

Imandra-Varzuga rohekivimite vöönd (*Imandra-Varzuga Greenstone Belt-IVGB*) paikneb Fennsokandia kilbi kirde osas, Loode Venemaal Koola poolsaarel. IVGB unikaalse geoloogilise läbilõike moodustavad kuni 3 km paksused vulkaaniliste ja settekivimite kompleksid, sealhulgas hästi säilinud murenemisprofiilid, mis stratigraafiliselt esindavad ajaperioodi, kus atmosfääri ilmus vaba hapnik. Nimetatud kivimite kompleksid võimaldavad meil selgitada hapnikulise atmosfääri tekkimise mõju kontinentaalsele murenemisele.

Käesoleva doktoritöö eesmärgiks oli hinnata murenemise intensiivsust ja keskkonnatingimusi (keskmine sademete hulk ja temperatuur) ja CO_2 kontsentratsioon Kuksha paleomurenemiskooriku kujunemise ajal 2,5 – 2,44 miljardit aastat tagasi ning hinnata kontinentaalse murenemise intensiivsuse muutuseid enne ja pärast hapnikulise atmosfääri kujunemist, kasutades IVGB geoloogilise läbilõike Seidorechka, Polisarka ja Umba kihistute savikiltade koostise analüüse. Doktoritöös kasutatud geoloogiline materjal pärineb 2007. aastal rahvusvahelise kontinentaalse puurimisprojekti „Fennoscandian Arctic Russia- Drilling Early Earth – FAR-DEEP“ raames puuritud puursüdamikest, mille läbilõigetes avatud kivimid katavad stratigraafiliselt 2 – 2,5 miljardi aasta taguse ajavahemiku.

Doktoritöö peamised tulemused näitavad, et vahetult enne hapnikulise atmosfääri tekkimist kujunenud Kuksha murenemiskooriku enim murenenud osa (ülemised 1,5–2 m) on keskmisest intensiivsemalt murenenud ja seda iseloomustavad kõrged murenemisindeksite CIA-K ja $MIA_{(R)}$ väärtused (vastavalt kuni 91 ja 45). Kõrge murenemisastmega on kooskõlas ka profiili ülaosas plagioklassi tüüpi päevakivide peaaegu täielik kadumine ja laialdane Al-rikaste savimineraalide esinemine. Erinevalt teistest Arhaikumi-Paleoproterosoikumi murenemiskoorikutest, mis on tüüpiliselt tugevalt mõjutatud hilisematest moondeprotsessidest, esineb Kuksha murenemiskoorikus endiselt kaoliniidi tüüpi savimineraale koos K-vilkude ning Fe-rikka kloriidiga. Viimased ilmselt esindavad vastavalt ümberkristalliseerunud Al-rikast smektiitset faasi ja Fe(II) -rikka vermikuliiti ja/või smektiiti.

Erinevaid paleotemperatuuride ja -sademete hindamismudelite alusel saab väita, et Kuksha murenemiskoorik kujunes jahedas lähistroopilises kliimas, kus aasta keskmine temperatuur oli ~12–13°C ja keskmine aastane sademete hulk 700–1100 mm/a, mis ligikaudu vastab tänapäevasele Vahemere piirkonna kliimale. Sellist paleokliima interpretatsiooni toetavad paleogeograafilised rekonstruktsioonid, mis viitavad, et Karjala kraaton paiknes 2,4 miljardi aasta eest

lõunapoolkera 30°–40° laiuskraadidel. Paleo-pH hinnangud näitavad Kuksha murenemiskooriku ülemises osas pH väärtuseks 5,0–5,5, mis on kooskõlas teiste happelisele murenemisele viitavate markeritega, nagu kõrge Ba/Sr suhe, kaoliniidi teke ja Cr leostumine.

Nii mass-tasakaalu kui ka stabiilsete isotoopide mudeli põhjal oli Kuksha murenemiskooriku tekkimise ajal hinnanguline paleoatmosfääri CO_2 osarõhk ainult 1–10 PAL (*Present Atmospheric Level* – võrrelduna tänapäevase atmosfääriga). Tüüpiliselt on hinnatud, et Eelkambriumi atmosfääri CO_2 osarõhk pidi olema enam kui 100 PAL, et hoida Maa keskmisi temperatuure üle külmumispiiri, sest päikesekiirguse intensiivsus oli Arhaikumi-Proterosoikumi piiril ligikaudu 20–25% nõrgem tänapäevasest. Samas Kuksha murenemiskoorik moodustus ajaperioodil, kui käivitus esimene globaalne Huroni jääaeg 2,46 – 2,426 miljardit aastat tagasi. Huroni jäätumiste algust seostatakse Kernolandi superkontinendi lagunemisel laialdaselt moodustnud basaltsete laavakatede murenemisega, mis põhjustas atmosfääri CO_2 taseme languse ning globaalse jahenemise.

Kuksha murenemiskoorikust stratigraafiliselt nooremate Paleoproterosoikumi Seidorechka, Polisarka ja Umba kihistute setendid Imandra-Varsuga rohekivimite vööndis on tõenäoliselt tekkinud kontinentaalsel riftistumisel avanenud basseinides. Seidorechka ja Polisarka kihistute setendite lähtekivimite hulgas domineerisid erinevad aluselised vulkaanilised kivimid. Seevastu stratigraafiliselt noorima Umba kihistu setendid pärinevad põhiosas korduvalt ümbertöötatud happelisema koostisega lähtekivimitest, mis võisid olla erodeerunud Polisarka kihistu vulkaanilisest kompleksist ja Arhaikumi graniit-gneissidest.

Murenemisindeksite väärtuste järgi on Imandra-Varsuga rohekivimite vööndi läbilõikes esindatud kolmest kihistust madalaima murenemise astmega Huroni jääajal moodustunud Polisarka terrigeensed setendid (keskmine CIA väärtus 57). Samas ei ilmnenud selget murenemisintensiivsuse erinevust Suurele Hapnikusündmusele eelnevates Seidorechka kihistu setendites (keskmine CIA 66) ja sellel järgnenud ajaperioodil eeldatavalt hapnikulistes tingimustes tekkinud Umba kihistu murenenud setendite (keskmine CIA 64) vahel.

Seega võib väita, et hapnikulise atmosfääri tekkimisega eeldatavalt sulfiidide oksüdeerumisega kaasnenud happelise murenemise impulss ei omanud märkimisväärset mõju üldisele silikaatide murenemise intensiivsusele. Olemasolevad andmed viitavad, et näiv murenemisintensiivsus Arhaikumi ja Proterosoikumi üleminekul pigem langeb koos atmosfääri CO_2 suhtelise sisalduse ja Maa pindmiste keskkondade agressiivsuse (sademete happelisuse) vähenemisega, millega tõenäoliselt kaasnes üldine kliima jahenemine.

ACKNOWLEDGEMENTS

I am most grateful to my supervisor Peeter Somelar for guidance and friendly help throughout my PhD, to Kalle Kirsimäe for keeping our data interpretations on the right path, and to Steven Driese for support and providing knowledge and practical skills for paleosol thin section analysis. I am also greatly thankful to my co-authors for their contribution that highly improved the quality of the research. I thank Aivo Lepland for providing us the samples and opportunities to additionally sample the cores ourselves. I am most thankful for having had this opportunity to work and spend time by discussing to arguing with the most interesting and lovely colleagues in Geology department at the University of Tartu. I thank Anne Noor for educated language correction.

This study was supported by the Estonian Research Council Grants (PUT1511, PUT696 and PRG447) and Archimedes Foundation (Kristjan Jaak and Dora Pluss) scholarships.

PUBLICATIONS

CURRICULUM VITAE

Name: Sigrid Soomer
Date of birth: 27.09.1986
Address: Department of Geology, University of Tartu,
Ravila 14A, 50411 Tartu, Estonia
Contact: +372 5557 4443
E-mail. sigrid.soomer@ut.ee

Education

2015–…	University of Tartu, Department of Geology, PhD student in geology
2017	PhD studies, Baylor University, Waco, Texsas, USA
2013–2015	University of Tartu, MSc in geology
2010–2013	University of Tartu, BSc in geology

Professional employment

2021–2022	Chemist in Geology, University of Tartu, Department of Geology
2018–2021	Specialist in Geology, University of Tartu, Department of Geology
2012–2015	Field Geologist

Field of research:
Archean-Paleoproterozoic transition, geochemistry, paleoweathering, paleoclimate

Publications:

Soomer, S., Somelar, P., Mänd, K., Driese, S. G., Lepland, A., Kirsimäe, K. (2019). High-CO2, acidic and oxygen-starved weathering at the Fenno-scandian Shield at the Archean-Proterozoic transition. *Precambrian Research*, 327, 68–80. https://doi.org/10.1016/j.precamres.2019.03.001

Somelar, P., Soomer, S., Driese, S. G., Lepland, A., Stinchcomb, G. E., Kirsi-mäe, K. (2020). CO2 drawdown and cooling at the onset of the Great Oxi-dation Event recorded in 2.45 Ga paleoweathering crust. *Chemical Geology*, 548, 119678. https://doi.org/10.1016/j.chemgeo.2020.119678

Soomer, S., Somelar, P., Mänd, K., Lepland, A., Kirsimäe, K. (2022). Geo-chemistry and mineralogy of Paleoproterozoic metasediments in the Imandra-Varzuga Greenstone Belt: implications for sediment provenance, tectonic settings and weathering intensity at the transition to oxygenated surface environments. *Precambrian Research*, 371, 106578. https://doi.org/10.1016/j.precamres.2022.106578.

ELULOOKIRJELDUS

Nimi: Sigrid Soomer
Sünniaeg: 27.09.1986
Aadress: Geoloogia osakond, Tartu Ülikool,
Ravila 14A, 50411 Tartu, Eesti
Kontakt: +372 5557 4443
E-post: sigrid.soomer@ut.ee

Haridus

2015–…	Tartu Ülikool, Geoloogia osakond, Geoloogia doktorant
2017	Doktoritöö teostamine välislaboris, Baylor University, Waco, Texsas, USA
2013–2015	Tartu Ülikool, MSc geoloogias
2010–2013	Tartu Ülikool, BSc geoloogias

Teenistuskäik

2021-2022	Tartu Ülikool, Geoloogia osakond, geoloogia keemik
2018-2021	Tartu Ülikool, Geoloogia osakond, geoloogia spetsialist
2012-2015	Välitööde geoloog

Teadustöö põhisuunad:
Archaikumi-Paleoproterozoikumi piiri sündmused, geokeemia, paleomullad, paleokliima

Publikatsioonid:

Soomer, S., Somelar, P., Mänd, K., Driese, S. G., Lepland, A., Kirsimäe, K. (2019). High-CO2, acidic and oxygen-starved weathering at the Fenno-scandian Shield at the Archean-Proterozoic transition. *Precambrian Research*, 327, 68–80.

Somelar, P., Soomer, S., Driese, S. G., Lepland, A., Stinchcomb, G. E., Kirsimäe, K. (2020). CO2 drawdown and cooling at the onset of the Great Oxidation Event recorded in 2.45 Ga paleoweathering crust. *Chemical Geology*, 548, 119678.

Soomer, S., Somelar, P., Mänd, K., Lepland, A., Kirsimäe, K. (2022). Geochemistry and mineralogy of Paleoproterozoic metasediments in the Imandra-Varzuga Greenstone Belt: implications for sediment provenance, tectonic settings and weathering intensity at the transition to oxygenated surface environments. *Precambrian Research*, 371, 106578. https://doi.org/10.1016/j.precamres.2022.106578.

DISSERTATIONES GEOLOGICAE UNIVERSITATIS TARTUENSIS

1. **Пээп Мянник.** Конодонты в верхнеордовикских и нижнесилурийских отложениях Эстонии. Тарту, 1992, 355 с.
2. **Elvi Tavast.** Fennoskandia kilbi lõunanõlva ja sellega piirnevate alade aluspõhja reljeef. Tartu, 1992, 357 lk.
3. **Kaarel Orviku.** Characterisation and evolution of Estonian seashores. Tartu, 1992, 19 p.
4. **Анатолий Молодьков.** ЭПР-анализ скелетного вещества моллюсков в хроностратиграфических исследованиях позднего кайнозоя. Тарту, 1992, 33 с.
5. **Jaan Lutt.** Late- and postglacial deposits on the Estonian shelf. Tartu, 1993, 31 p.
6. **Reet Karukäpp.** Gotiglatsiaalne morfogenees Skandinaavia mandriliustiku kagusektoris. Tartu, 1997, 181 p.
7. **Argo Jõeleht.** Geothermal studies of the Precambrian basement and Phanerozoic sedimentary cover in Estonia and Finland. Tartu, 1998, 125 p.
8. **Jüri Nemliher.** Mineralogy of Phanerozoic skeletal and sedimentary apatites: an XRD study. Tartu, 1999, 134 p.
9. **Kalle Kirsimäe.** Clay mineral diagenesis on the Lower Cambrian "Blue Clay" in the northern part of the Baltic Paleobasin. Tartu, 1999, 113 p.
10. **Jüri Plado.** Gravity and magnetic signatures of meteorite impact structures. Tartu, 2000, 87 p.
11. **Olev Vinn.** Morphogenesis and phylogenetic relationships of Clitambonitidines, Ordovician Brachiopods. Tartu, 2001, 127 p.
12. **Leho Ainsaar.** The middle Caradoc facies and faunal turnover in the late Ordovician Baltoscandian palaeobasin: sedimentological and carbon isotope aspects. Tartu, 2001, 109 p.
13. **Oive Tinn.** Early Ostracode evolution and Palaeoenvironmental application in the Ordovician of Baltoscandia. Tartu, 2002, 145 p.
14. **Maris Rattas.** Subglacial environments in the formation of drumlins — The case of the Saadjärve Drumlin Field, Estonia. Tartu, 2004, 117 p.
15. **Ene Kadastik.** Upper-Pleistocene stratigraphy and deglaciation history in northwestern Estonia. Tartu, 2004, 129 p.
16. **Helje Pärnaste.** Early Ordovician trilobites of suborder Cheirurina in Estonia and NW Russia: systematics, evolution and distribution. Tartu, 2004, 138 p.
17. **Mari-Ann Mõtus.** Silurian (Llandovery-Wenlock) tabulate corals of Baltoscandia: taxonomy, palaeoecology, distribution. Tartu, 2005, 167 p.
18. **Alar Rosentau**. Development of proglacial lakes in Estonia. Tartu, 2006, 114 p.
19. **Evelin Verš.** Development of impact-induced hydrothermal system at Kärdla impact structure. Tartu, 2006, 96 p.

20. **Sigitas Radzevičius.** The genus *Pristiograptus* in wenlock of East Baltic and the Holy Cross Mountains. Tartu, 2007, 133 p.
21. **Andres Marandi.** Natural chemical composition of groundwater as a basis for groundwater management in the Cambrian-Vendian aquifer system in Estonia. Tartu, 2007, 116 p.
22. **Eve Niinemets.** Vegetation and land-use history of the Haanja Heights (SE-Estonia) during the holocene. Tartu, 2008, 146 p.
23. **Kalle-Mart Suuroja.** Geology and lithology of the early palaeozoic marine impact stuctures Kärdla and Neugrund (Estonia). Tartu, 2008, 234 p.
24. **Rutt Hints.** Early diagenesis of Ordovician and Silurian Bentonites in the Northern Baltic Palaeobasin. Tartu, 2009, 90 p.
25. **Peeter Somelar.** Illitization of K-bentonites in the Baltic Basin. Tartu, 2009, 118 p.
26. **Ulla Preeden.** Remagnetizations in sedimentary rocks of Estonia and shear and fault zone rocks of southern Finland. Tartu, 2009, 121 p.
27. **Kati Tänavsuu-Milkeviciene.** Transgressive to regressive turnaround in the Middle Devonian Baltic Basin. Tartu, 2009, 106 p.
28. **Valle Raidla.** Chemical and isotope evolution of groundwater in the Cambrian-Vendian aquifer system in Estonia. Tartu, 2010, 134 p.
29. **Kadri Sohar.** Quaternary ostracods from Estonia and their application in palaeoenvironmental reconstruction. Tartu, 2010, 140 p.
30. **Kristjan Urtson.** Stepwise melt transport and accumulation: analogue and numerical modelling approach. Tartu, 2011, 83 p.
31. **Marko Kohv.** Landslides in clayey soils of western Estonia. Tartu, 2011, 116 p.
32. **Nele Muttik.** Post-impact alteration of impactites: Ries crater, Germany. Tartu, 2011, 78 p.
33. **Annette Sedman.** Strength and self-cementing properties of oil shale retorting wastes. Tartu, 2013, 82 p.
34. **Arkady Tsyrulnikov.** Complex seismo-acoustic and lithological study of the Lateglacial and postglacial sediments northern Gulf of Riga, eastern branch of the central Baltic Sea. Tartu, 2013, 102 p.
35. **Marge Uppin.** Geological sources and hydrochemistry of fluoride and boron in Silurian-Ordovician aquifer system. Tartu, 2013, 86 p.
36. **Peeter Talviste**. Temporal changes in weak natural and artificial soils – influence on geotechnical characteristics. Tartu, 2014, 204 p.
37. **Katrin Lasberg.** Chronology of the Weichselian Glaciation in the south-eastern sector of the Scandinavian Ice Sheet. Tartu, 2014, 100 p.
38. **Sirle Liivamägi.** Neoproterozoic Baltic paleosol: geology and paleoenvironmental interpretation. Tartu, 2015, 94 p.
39. **Lauri Joosu.** Petrography and the rare earth element composition of apatite in 2 Ga Onega and Pechenga basins, Russia: the environmental settings for phosphogenesis. Tartu, 2015, 139 p.
40. **Liisa Lang.** Baculate shell structure in Early Palaeozoic linguliform brachiopods. Tartu, 2015, 114 p.

41. **Päärn Paiste.** Geopolymeric potential of the Estonian oil shale processing waste. Tartu, 2017, 125 p.
42. **Mikk Gaškov.** Stable isotope and fluid inclusion evidence of multistage fluidal activity in Baltic paleobasin: Silurian carbonate sequence in Kalana, Estonia. Tartu, 2017, 104 p.
43. **Viirika Mastik.** Silurian noncalcified macroscopic algal fossils from the Kalana *Lagerstätte*, Estonia. Tartu, 2018, 91 p.
44. **Kairi Põldsaar.** Soft-sediment deformation and gravity flow structures in the Lower Palaeozoic successions of the Baltic Basin. Tartu, 2019, 105 p.
45. **Timmu Kreitsmann.** Application of carbon isotope and rare earth elements as recorders of environmental conditions in the aftermath of the Paleoproterozoic Lomagundi-Jatuli Event. Tartu, 2020, 163 p.
46. **Triine Nirgi.** Holocene relative shore-level changes and geoarchaeology of the prehistoric sites in western Estonia. Tartu, 2020, 161 p.
47. **Kristjan Leben.** Long-term diagenetic transformation and carbon sequestration potential of Ca-rich oil shale ash waste deposit sediments. Tartu, 2021, 117 p.
48. **Karin Truuver.** Ostracod associations of the ordovician–silurian boundary interval in baltoscandia. Tartu, 2021, 132 p.
49. **Kaarel Lumiste.** Phosphogenesis and REE+Y diagenesis of Recent and Paleozoic phosphorites. Tartu, 2021, 174 p.